

**SURFACE MODIFICATION OF ALUMINIUM ALLOY
SERIES 6 (AA6061 T657) AND ITS CORROSION
CHARACTERISTICS**

CHRISTOPHER TSEU ZIA CHYUAN

**FACULTY OF ENGINEERING
UNIVERSITY OF MALAYA
KUALA LUMPUR**

2019

**SURFACE MODIFICATION OF ALUMINIUM ALLOY
SERIES 6 (AA6061 T657) AND ITS CORROSION
CHARACTERISTICS**

CHRISTOPHER TSEU ZIA CHYUAN

**THESIS SUBMITTED IN FULFILMENT OF THE
REQUIREMENTS FOR THE DEGREE OF MASTER OF
MECHANICAL ENGINEERING**

**FACULTY OF ENGINEERING
UNIVERSITY OF MALAYA
KUALA LUMPUR**

2019

UNIVERSITY OF MALAYA
ORIGINAL LITERARY WORK DECLARATION

Name of Candidate: Christopher Tseu Zia Chyuan

Matric No: KQK 160026

Name of Degree: Master of Mechanical Engineering

Title of Project Paper/Research Report/Dissertation/Thesis (“this Work”): “Surface Modification of Aluminium Alloy Series 6 (AA6061 T657) and Its Corrosion Characteristics”

Field of Study: Nanomaterials / Advance Materials

I do solemnly and sincerely declare that:

- (1) I am the sole author/writer of this Work;
- (2) This Work is original;
- (3) Any use of any work in which copyright exists was done by way of fair dealing and for permitted purposes and any excerpt or extract from, or reference to or reproduction of any copyright work has been disclosed expressly and sufficiently and the title of the Work and its authorship have been acknowledged in this Work;
- (4) I do not have any actual knowledge nor do I ought reasonably to know that the making of this work constitutes an infringement of any copyright work;
- (5) I hereby assign all and every rights in the copyright to this Work to the University of Malaya (“UM”), who henceforth shall be owner of the copyright in this Work and that any reproduction or use in any form or by any means whatsoever is prohibited without the written consent of UM having been first had and obtained;
- (6) I am fully aware that if in the course of making this Work I have infringed any copyright whether intentionally or otherwise, I may be subject to legal action or any other action as may be determined by UM.

Candidate’s Signature

Date:

Subscribed and solemnly declared before,

Witness’s Signature

Date:

Name:

Designation:

ABSTRACT

Aluminium (Al) casting alloys are important materials for the fabrication of engine components such as engine block, cylinder head and piston rings. In the present study, a self-organized nanostructured Al₂O₃ layer on AA6061 T657 series was fabricated by anodization followed by heat treatment at 450 °C for 1.5 h. The microstructural features and surface wettability were explored. In addition, mechanical and corrosion behavior of Al₂O₃ nanoporous after anodizing and annealing were investigated. From the microstructural point of view, the average length and diameter of the optimized nanoporous arrays ranged from 0.5 μm and 25 nm. The adhesion results showed that the adhesion strength of coating increased for un-treated substrate from 1532 mN to annealed sample of 2240 mN. To improve the hardness of Al, heat treatment was carried out at 450 °C for 1 hour which returned with a hardness value of 71.2 as compared to substrate at 45.9. Besides, the annealed coating showed that highest wettability (lowest contact angle value). The results of corrosion tests in artificial sea water (ASW) showed that the corrosion rate values significantly decreased after anodization and subsequent annealing compared to the substrate

Keywords: AA6061 T657; Anodization; Tribocorrosion; Wettability; Mechanical properties.

ABSTRAK

Aluminium (Al) adalah bahan penting untuk fabrikasi komponen engine seperti blok mesin, piston, dan kepala silinder. Dalam kajian ini, lapisan Al_2O_3 nanostruktur yang tersusun sendiri pada siri AA6061 T657 direka dengan anodisasi dan diikuti oleh rawatan haba pada suhu $450\text{ }^\circ\text{C}$ selama 1.5 jam. Ciri-ciri mikrostruktur dan kelembapan permukaan telah diterokai. Di samping itu, kelakuan mekanikal dan kakisan Al_2O_3 nanostruktur selepas anodisasi dan rawatan haba disiasat. Dari sudut pandangan mikrostruktur, panjang purata dan diameter garis nanostruktur yang dioptimumkan adalah $0.5\text{ }\mu\text{m}$ dan 25 nm . Keputusan lekatan menunjukkan bahawa kekuatan lekatan salutan meningkat untuk substrat yang tidak dirawat dari 1532 mN ke sampel rawatan haba 2240 mN . Untuk meningkatkan kekerasan Al, rawatan haba dilakukan pada suhu $450\text{ }^\circ\text{C}$ selama 1 jam yang dikembalikan dengan nilai kekerasan 71.2 HV berbanding dengan substrat pada 45.9 HV . Selain itu, salutan rawatan haba menunjukkan bahawa kebolehdayaan kelembapan permukaan (nilai sudut kontak terendah). Hasil ujian kakisan dalam air laut buatan menunjukkan bahawa kadar hakisan berkurang dengan ketara setelah anodisasi dan rawatan haba berbanding dengan substrat.

Keywords: AA6061 T657; Anodisasi; Tribokakistan; Kelembapan; Sifat Mekanikal

ACKNOWLEDGEMENTS

I would like to acknowledge Dr. Nazatul Liana Binti Sukiman and Dr. Masoud Sarraf for their invaluable guidance and generous support throughout the research project for making this achievable. Dr. Nazatul for giving me the opportunity to further my research work in the field of advance materials, while Dr. Masoud Sarraf for guiding me whenever I have difficulty in interpreting the results and rendering help whenever I have difficulty in performing certain experiments.

I would also express my gratitude to my family especially my parents for their unconditional moral support and unending encouragement in making this possible by accomplishing my postgraduate study in University Malaya. Last but not least, sincere appreciation to lab technicians for their help, and generosity in sharing their knowledge and expertise for making this research possible.

TABLE OF CONTENTS

Abstract	iii
Abstrak	iv
Acknowledgements.....	1
Table of Contents.....	2
List of Figures.....	5
List of Tables.....	7
List of Symbols and Abbreviations	8
CHAPTER 1: INTRODUCTION.....	9
1.1 Background Study	9
1.2 Problem Statement.....	12
1.3 Aim and Objectives	13
1.4 Research Scope.....	13
1.5 Thesis Outline.....	14
CHAPTER 2: LITERATURE REVIEW	16
2.1 Introduction	16
2.2 Aluminium and Its Alloys.....	16
2.3 Self-Organized Systems – Aluminium Oxides Template	17
2.3.1 Barrier Oxides.....	19
2.3.2 Nanoporous Oxides.....	20
2.3.3 Synthesis Techniques of Anodic Aluminium Oxide Template	21
2.3.3.1 Anodization.....	22
2.4 Formation Mechanism of Alumina Nanoporous.....	24
2.5 Processing Parameters Effects on the Development of Porous Alumina	26

2.5.1	Effects of Anodization Voltage to the Formation of Anodic Aluminium Oxide	26
2.5.2	Effects of Anodization Surface on the Formation of Anodic Aluminium Oxide	27
2.5.3	Effects of Anodization Electrolyte to the Formation of Anodic Aluminium Oxide	27
2.6	Other Anodic Metal Oxides	28
2.6.1	Anodization of Niobium.....	28
2.6.2	Anodization of Tungsten.....	29
2.6.3	Anodization of Titanium	30
2.6.4	Anodization of Zirconium	30
2.6.5	Anodization of Tantalum.....	31
2.7	Two-Step Anodization of Aluminium	32
2.7.1	Hardness of Al and Al ₂ O ₃ Nanoporous.....	33
2.7.2	Wettability of Al and Al ₂ O ₃ Nanoporous	34
2.7.3	Corrosion of Al and Al ₂ O ₃ Nanoporous.....	34
2.8	Heat treatment of Al and Al ₂ O ₃ Nanoporous	34
CHAPTER 3: MATERIALS, METHODS AND PROCEDURES.....		36
3.1	Substrate Preparation	38
3.2	Preparation of Self-Organized Al ₂ O ₃ Nanoporous Arrays	40
3.3	Annealing	41
3.4	Characterization Techniques	42
3.4.1	Field Emission Scanning Electron Microscope.....	42
3.4.2	X-Ray Diffractometry	42
3.4.3	Energy Dispersive X-Ray Spectroscopy	43
3.5	Adhesion Strength	43

3.6	Microhardness	44
3.7	Corrosion Studies	45
3.8	Surface Wettability	46
CHAPTER 4: RESULTS AND DISCUSSION		48
4.1	XRD Analysis.....	48
4.2	Microstructure of Al ₂ O ₃ Nanoporous Array after Anodization	49
4.3	Adhesion Strength of Al ₂ O ₃ Nanoporous Array and Heat Treated	52
4.4	Vickers Microhardness	57
4.5	Effectiveness of Corrosion Protection	58
4.6	Surface Wettability	60
CHAPTER 5: CONCLUSION AND FUTURE WORK.....		63
5.1	Conclusion.....	63
5.2	Suggestions for Future Work	64
REFERENCES		65

LIST OF FIGURES

Figure 1.1: Flow of project activities.....	15
Figure 2.1: Formation of aluminium oxide (top) and aluminium oxide thin film (below) via anodization.....	17
Figure 2.2: Side view of amorphous oxide layer (top) laminated on Al metal substrate (bottom)	19
Figure 2.3: Evolution of AAO template substrates during anodization at fixed voltage.....	20
Figure 2.4: SEM view (left) and cross-sectional view (right) of perfect hexagonal anodic porous alumina oxide layer	24
Figure 2.5: Growth formation of porous AAO.....	25
Figure 2.6: Porous Nb ₂ O ₅ (a) view and (b) side view anodized in 1 M H ₂ SO ₄ + 0.2 wt% NaF	27
Figure 2.7: Porous WO ₃ (a) view and (b) side view anodized at 10 V and 35 V	28
Figure 2.8: Porous ZrO ₂ (a) view and (b) side view	29
Figure 2.9: Porous Ta ₂ O ₅ (a) view and (b) side view.....	29
Figure 2.10: Schematic of two-step anodization process involving (a) electropolished surface, (b) first anodization, (c) oxide removal, and (d) second anodization.....	30
Figure 3.1: Schematic diagram of nanoporous anodic alumina on AA6061 metal.....	33
Figure 3.2: AA6061 T657 plates after cutting into smaller plates.....	34
Figure 3.3: Grinder and polisher machine.....	35
Figure 3.4: Ultrasonic cleaning bath.....	35
Figure 3.5: Electrochemical anodization process to produce Al ₂ O ₃ nanoporous array....	36
Figure 3.6: Furnace for annealing of substrate.....	37
Figure 3.7: Schematic of scratch hardness measurement	40
Figure 4.1: XRD profiles of the (a) bare substrate, (b) the anodized sample, and (c) the heat treated sample at 450 °C for 1.5 h.....	47

Figure 4.2: (a) Top view FESEM image and (b) EDX analysis of AA6061 series 6 substrate.....	48
Figure 4.3: (a) FESEM top-view image and (b) EDX analysis of Al ₂ O ₃ nanoporous array after anodization for 1 h at 12 V in 15 wt% H ₂ SO ₄	49
Figure 4.4: FESEM cross-sectional image of Al ₂ O ₃ nanoporous array after anodization process for 1 h in an electrolyte containing 15 wt% H ₂ SO ₄ at 12 V.....	50
Figure 4.5: The optical micrograph of scratch track and graph profiles of (b) depth, (c) load, (d) friction, and (e) COF against scan distance inclusive of failure points of the 1 h anodized specimen.....	53
Figure 4.6: The optical micrograph of scratch track and graph profiles of (b) depth, (c) load, (d) friction, and (e) COF against scan distance inclusive of failure points for anodized sample after thermal heat treatment at 450 °C.....	54
Figure 4.7: Vickers hardness value of (a) substrate, (b) anodization in 15 wt% H ₂ SO ₄ and (c) heat treatment at 450 °C.....	56
Figure 4.8: Polarization plots of the untreated substrate, the anodized specimen, and the 450 °C heat-treated sample	58
Figure 4.9: Optical image of the contact angle of (a) substrate, (b) anodized in H ₂ SO ₄ electrolyte, and (c) heat treated sample at 450 °C.....	60

LIST OF TABLES

Table 1.1: Chemical composition suitable for casting automotive components.....	10
Table 2.1: Electrolyte composition coating on aluminium alloys.....	23
Table 4.1: Corrosion potential (E_{Corr}), corrosion current density (I_{Corr}), corrosion rate and effectiveness of corrosion protection ($P.E.$) values	59

University of Malaya

LIST OF SYMBOLS AND ABBREVIATIONS

For examples:

AA	:	Aluminium alloy
AFM	:	Atomic force microscopy
AAO	:	Anodic aluminium oxide
ASW	:	Artificial sea water
COF	:	Coefficient of friction
EDX	:	Field emission scanning electron microscopy
E_{Corr}	:	Corrosion potential
FESEM	:	Field emission scanning electron microscopy
I_{Corr}	:	Corrosion current density
PAO	:	Porous anodic oxide
P.E.	:	Corrosion protection
R_{P}	:	Polarization resistance
XRD	:	X-ray photoelectron microscopy

CHAPTER 1: INTRODUCTION

1.1 Background Study

The first successfully working internal combustion engine (ICE) employed in the automotive industry was discovered by Siegfried Marcus in the year 1864 (Landmark, 2005). Back then, most of the engine blocks were manufactured from steel metal and cast iron primarily due to its low cost, good mechanical properties and availability. Over the past couple of years, aluminium metal has been the preferred material in the aerospace, marine, gasoline and diesel-powered engine block in the automotive industry. As time goes on, more stringent requirements to tackle carbon footprint emitted by vehicle exhaust emissions and also to improve occupant safety, automotive manufacturers are making efforts to develop newer drivetrain, while improving the conventional engine efficiency. From there on, automakers also seek to improve gas mileage by utilizing lighter components materials with the use of aluminium alloy. Due to modernization and the complexity of automotive engines, aluminium alloy has been the forefront for the transport and automotive industry and is expected a compound annual growth rate (CAGR) of 7.8% by the year 2023 (Research and Markets, 2018).

The patent developed by General Motors shows the desired combine material comprises, by weight in Table 1.1, with the balance in aluminium provides good castability, wear resistance and corrosion resistance in automotive components while fulfilling the lightweight criteria which will enhance the manufacturing and performance for cylinder block and piston on the cylinder walls (United States Patent No. US 6,921,512 B2, 2005). According to Miller *et al.*, the use of aluminium castings in automotive have seen significant increase in application and have been used and substituted with cast iron for approximately three-fourth of total cylinder heads, 100% of pistons, 85% of intake manifolds transmissions, drive shafts and differential housings. On

top of that, aluminium castings used for chasis application accounts 40% of the brake components, suspensions, disc wheel, steering shaft and components (Miller, et al., 2000). This shows that aluminium will enhance the manufacturing and performance for cylinder block and piston/ring on the cylinder walls and the combination of aluminium and alloy produces a versatile metallic material to be used ranging from structural metals to demanding engineering applications

Table 1.1: Chemical composition suitable for casting automotive components
(United States Patent No. US 6,921,512 B2, 2005)

Component	(Wt.%)
Nickel	0 – 1.5
Copper	1.5 – 4.5
Magnesium	0.1 – 0.6
Silicon	9.5 – 12.5
Iron	0.1 – 1.5
Manganese	0.2 – 3.0
Titanium	Max 0.25
Zinc	Max 2.0
Strontium	Up to 0.05

Development of wrought aluminium is also employed in the field of heat exchanger conducted by Toyota Motor Corporation, which uses brazed aluminium-tube structure in the radiator as opposed to the conventional copper-tube structure. Fin material is also switched in the radiator to prevent corrosion (Morita, 1998).

Recently, a research shows the creation of low specific weight and wettability behavior found on aluminium surface provides a multitude of application especially in

the field of tribology and corrosion (Rodrigues, 2017). In addition to that, there are various external factor which also influences the mechanical and tribological characteristics of aluminium and its alloys, for instance the size, shape, nature and distribution of micro-constituents (Prasad B.K, 1998).

Research steered by Li *et al.* showed that the fabrication of aluminium through rolling process are often subjected to shear strain and deformation, which deforms the microstructure near-surface layer. This may influence the optical properties and electrochemical response (Li *et al.*, 2013). Huttunen-Saarivirta have studied that the behavior of aluminium alloy also changes especially at elevated temperature making it more prone to oxidation on the surface process (Dohda *et al.*, 2015). It was also found that the corrosion behavior of aluminium alloy also affects the near-surface deformed layer due to finer grains (Liu *et al.*, 2017). The performance of aluminium alloy relies mostly on the size and dispersion of silicon phase, nature of attachment between the lattice and silicon, and silicon fracture characteristic (Anand S, 1997).

Aluminium in general projects good resistance towards corrosion when exposed to aqueous and atmosphere environment as opposed to steel, prominently due to the formation of resistive native amorphous oxide film (Revie, 2008). As described by Nayak, aluminium alloy is seen as one of the potential metallic materials suitable for various applications, if appropriate surface technology is employed to improve its characteristics (Nayak, 2004). Hence, due to wide application of aluminium and its alloys in various systems, extensive study was done.

In the present study, the lamination of alumina was deposited on the AA 6061 substrate via anodization. The effect of anodization and dissolution reactions on the structural and material properties over fixed current densities and electrolyte temperature was investigated.

1.2 Problem Statement

Aluminium alloy are often used in various engineering applications due to their light weight, high strength-to-weight ratio, ease of fabrication and resistance to corrosion (Kucharikova *et al.*, 2018). On top of that, aluminium has been the second favorable properties used for automobile manufacturing according to Aluminium Association (Association, 2018). However, in order to reduce the risk of corrosion, further improvements in surface properties are required to integrate aluminium and its alloys into the production of automotive. Hence the study of corrosion properties of aluminium will be of vital importance to understand the effect of microstructural arrangement on the corrosion resistance of aluminium.

Besides that, more stringent requirements by using aluminium alloy to tackle carbon footprint emitted by vehicle exhaust emissions and also to improve occupant safety, automotive manufacturers are making efforts to develop newer drivetrain, while improving the conventional engine efficiency. Vehicle weight has direct impact on fuel efficiency and emissions as it uses more energy and fuel to propel forward as opposed to a lighter vehicle. By using aluminium, the vehicle weight of the car can be reduced to 40% as compared to using steel alone (Association, 2018).

However, higher loads from the mixture of internal combustion engine leads to higher stress and thermal heat, in the advent leading to catastrophic failure. Poor surface properties have severely impacted its economic advantages over other ferrous materials. For future, mechanical properties of aluminium alloy will be studied in depth along the project.

1.3 Aim and Objectives

This study aims to develop non-porous surface aluminium alloy, AA6061-T6 to improve their tribological characteristic, corrosion resistance and mechanical properties. The synthesis of aluminium alloy oxide (AAO) template is developed with similar substrates via anodization process. This project aims to achieve a few objectives;

1. To fabricate aluminium oxide non-porous layer by application of surface modification, which is anodization and heat treatment
2. To investigate the corrosion behavior of AA6061 and effect of surface modification on its corrosion behavior in artificial salt water through experimental methods and microstructure analysis

1.4 Research Scope

The aim to this current study is to investigate the type of parameters controlling corrosion in aluminium alloy, AA6061-T6. The project also focuses on ways to optimize the anodization and heat treatment methods in order to obtain aluminium alloy oxides (AAO) template on the substrates with enhanced material, tribological and corrosion resistance. The proposed aluminium alloy metal, AA6061 will be tested in the laboratory to determine the corrosion by surface modification. The morphological properties will be investigated using field emission scanning electron microscopy (FESEM) combined with energy dispersive spectroscopy (EDS) while the developed thin film will also undergo X-ray diffractometry (XRD). The chemo-mechanical performance of AAO was also evaluated by wear, adhesion, corrosion, and microhardness test.

1.5 Thesis Outline

In this current chapter, a brief introduction of the project was presented, and the current challenges addressed in this project were explored. The scope of this study was outlined, and the research objectives were clarified based on the existing limitations.

In chapter 2, a detailed background study in the mechanical performance of AAO template on the AA6061-T657 substrate is presented. The chapter also covers the detailed approach, starting from the initial fabrication phase towards the final product evaluation while highlighting the critical parameters in order to achieve the desired mechanical, and morphological properties.

Chapter 3 highlights the methodology employed for preparation of AAO templates on AA6061-T6 substrates, starting from substrate preparation, anodization, annealing, as well as the characterization approach employed for investigation of mechanical, tribological and morphological properties of the formed coatings.

Chapter 4 analyzed the results of various sample characteristics of the developed AAO template layer. Aside from that, the chapter also discusses the formation procedures of oxide films. Optimum anodizing parameters, including anodization voltage, anodizing time and electrolyte concentrations are suggested.

Finally, chapter 5 concludes the obtained results and recommendations to improve the area of research in future studies. The flow of project activities is summarized below in Figure 1.1.

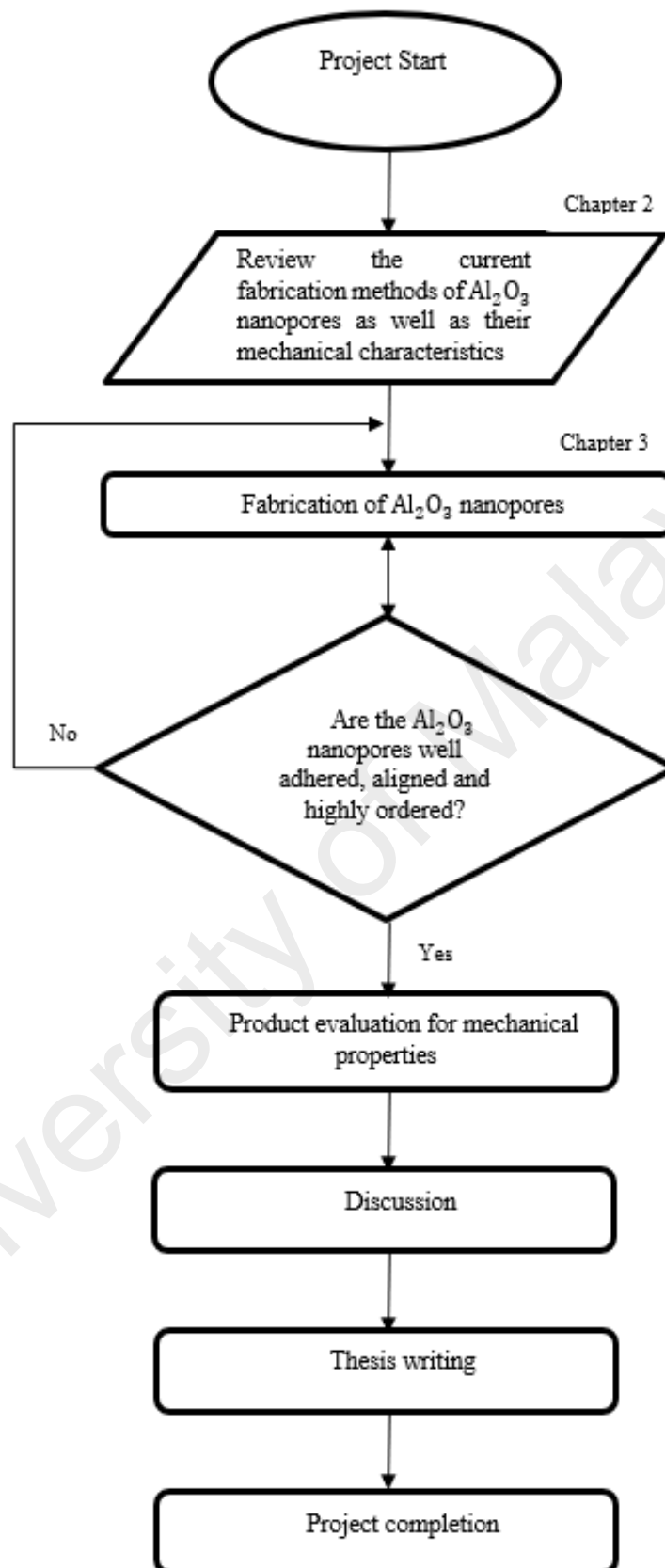


Figure 1.1: Flow of project activities

CHAPTER 2: LITERATURE REVIEW

2.1 Introduction

Anodization of aluminium and its alloys is one of the most important and widely used electrochemical process to produce a layer of coating for corrosion protection, surface finishing, decoration and improvement of mechanical properties on aluminium. Anodic films have also received large attention due to their extensive application in aerospace, architecture, automotive and functionalization of aluminium alloys such as nanostructure and nanopores (El-Hameed *et al.*, 2017). Under typical atmospheric conditions, a great number of metals on the surface are naturally prone to the formation of native oxide film. Nevertheless, the lamination of native oxide film due to oxidation only provides corrosion protection up to a certain level (Fournier *et al.*, 2004). This chapter assess and review the current development of porous anodic oxide (PAO) films formation, along with the key attributes to a desirable coating deposition on substrate depending on several parameters will be reviewed.

2.2 Aluminium and Its Alloys

Aluminium is the third most abundant metal element in the Earth's crust, just after oxygen and silicon (Atkins & Paula, 2009). It is usually found in the oxide form known as bauxite and has been estimated that the aluminium represents 8 percent of the total earth crust. Aluminium in general has a density of 2.7 g/cm^3 , and is made up mostly of silicon and magnesium as its main principal alloying elements and is approximately 35% lighter as compared to steel metal with a density of 7.83 g/cm^3 . Material selection due to the formation of thin native oxide layer when exposed to atmospheric air, which prevents further oxidation provides excellent corrosion resistance. Aside from that, other valuable properties include good electrical and thermal conductivities, ductility, reflectivity, cost effective and nonferromagnetic characteristics (Xhanari & Finsgar, 2016).

2.3 Self-Organized Systems – Aluminium Oxides Template

As early in 1932, Miyata and Setoh had researched that the anodic aluminium oxide (AAO) template comprises of only two types of surface layers, a thin barrier layer attached on the aluminium substrate which results in a total thickness of less than 0.5-2% film and a porous outer layer as illustrated below in Figure 2.1 (Yudong, 2017).

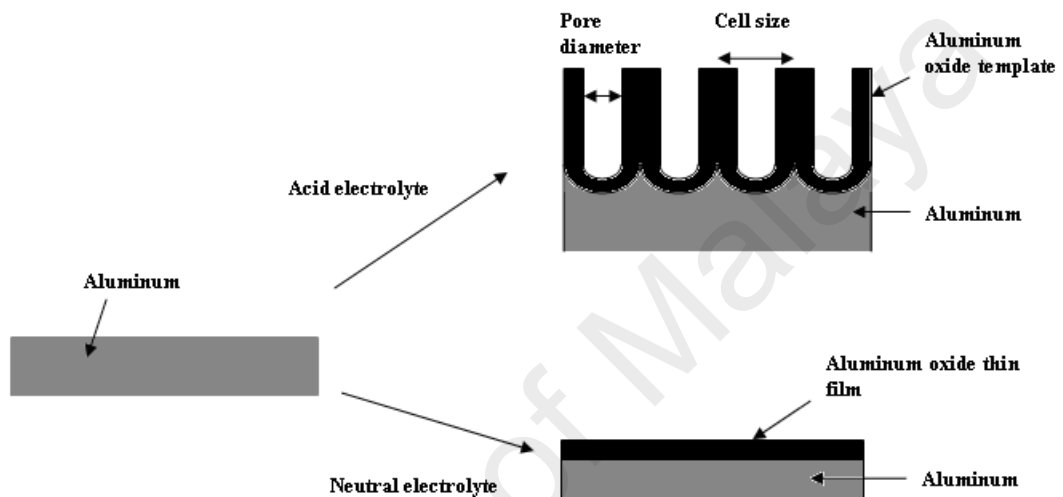


Figure 2.1: Formation of aluminium oxide (top) and aluminium oxide thin film (below) via anodization (Lim, 2011).

Anodization of aluminium were first discovered 50 years ago by Keller in 1953 (Keller *et al.*, 1953). The formation of compact aluminium oxide thin film is obtained using electrolytes with $\text{pH} > 5$ during anodization. As for the formation of AAO template with porous structure can only be produced by using acidic based electrolytes which will be discussed later at a later stage. The purpose of anodization has been widely used as aesthetic purpose and in application requiring protection to corrosion and wear. When aluminium is anodized in an aqueous electrolyte, either two types of aluminium oxides will be formed on the aluminium substrate, which is barrier and porous oxide films (Diggle *et al.*, 1968; Lee & Park, 2014).

Several studies concluded that various morphological of porous layer under tailored anodization results in layer having narrow pore size distribution and larger surface area (Diggle *et al.*, 1968). With the rapid development in scanning electron microscopy (SEM), O' Sullivan and Wood discovered a significant step in understanding the types of growth mechanisms of anodic alumina oxide layer in the 1980's (O'Sullivan & Wood, 1970).

From there onwards, subsequently porous anodic alumina oxide was further investigated, which leads to the formation of self-organized hexagonal structures consists of porous and layer barrier under various anodic electrolytes (Jessensky *et al.*, 1998). It was then reported by Masuda that for a certain set of parameters, e.g., applied voltage, electrolyte composition, electrode distance would affect the densely packed hexagonal pore structure growth. (Masuda & Hasegwa, 1997).

Continuous effort in the research of porous alumina leads to the success in growing highly ordered, well-adherent layers, known as honeycomb porous alumina by Japanese researchers (Masuda & Fukuda, 1995).

2.3.1 Barrier Oxides

Barrier oxide film comprises of compact, dense layer of amorphous oxide layer with a thickness of 1 μm and are generally developed in mild environments. This thin barrier oxide serves as the first defensive layer to prevent against oxidation. Generally, it is notable for its high activity when exposed to atmospheric surrounding. Aluminium can easily react with the atmosphere resulting in the lamination of boundary oxide layer of the aluminium surface as shown in Figure 2.2.

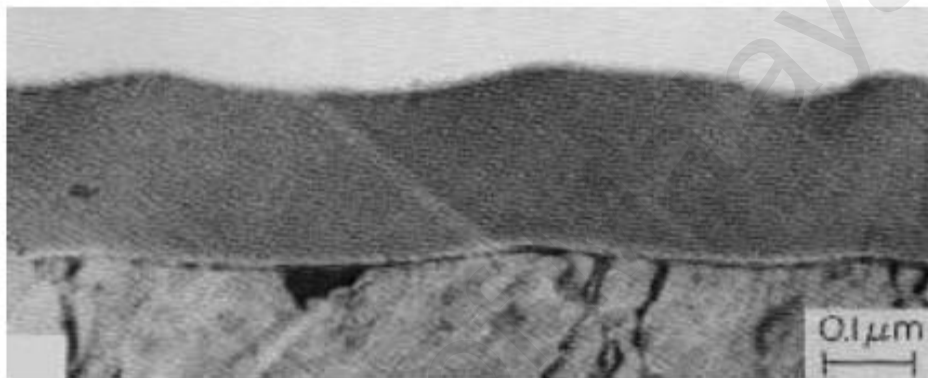


Figure 2.2: Side view of amorphous oxide layer (top) laminated on Al metal substrate (bottom) (Kikuchi *et al.*, 2013)

According to Kikuchi *et al.*, there is a connection link between the barrier oxide formation thickness, with the electrochemical potential employed to the aluminium substrate during anodization (Kikuchi *et al.*, 2015). It is said that constant current anodized in neutral pH electrolytes cause a linear increase with anodizing time, which ends the linear formation of oxide at higher current density, known as the ‘breakdown potential’. (Ikonopisov *et al.*, 1979; Yahalom & Hoar, 1970). The breakdown potential is also affected by the concentration and type of electrolytes used (Yi Li *et al.*, 1997).

Hence, due to the overwhelming properties of barrier AAO films, it is being investigated in great details by researchers due to its high dielectric property mainly employed in aluminium electrolytic capacitor (Uchi *et al.*, 2001; Du & Xu, 2008).

2.3.2 Nanoporous Oxides

Generally, AAO anodized in aqueous acid solutions such as sulphuric acid, phosphoric acid, chromic acid and oxalic acid will be further discussed. Unlike barrier type oxides, porous oxides form due to dissolution reactions. Figure 2.3 shows the development of anodic aluminium oxide (AAO) template substrates anodized at fixed voltage. A detailed review researched by Diggle *et al.*, on the progress of AA6061 anodization, from fabrication, to material characterization will be shared (Diggle *et al.*, 1968).

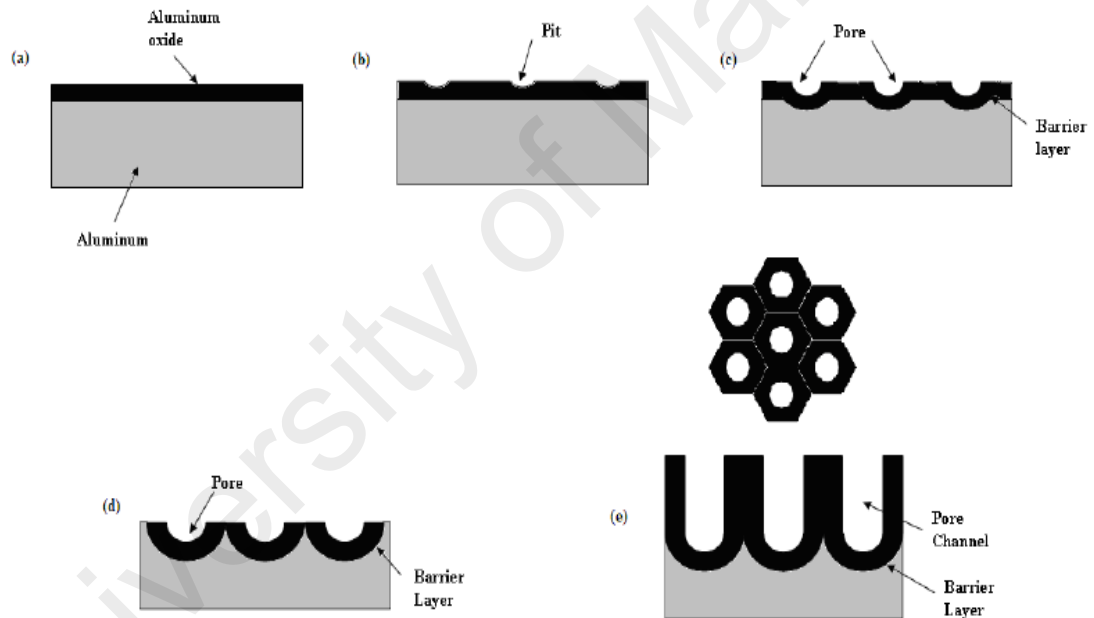


Figure 2.3: Evolution of AAO template substrates during anodization at fixed voltage

(Lim, 2011)

During the initial anodization stage, a thin oxide layer is shaped due to the interaction of Al^{3+} ions from Al surface as well as the O^{2-} ions present in the acid electrolyte. The O^{2-} ions derive from the water due to splitting. Subsequently, electrical field is formed on the metal/oxide boundary causing the Al^{3+} ions to migrate to the

electrolyte while the O^{2-} ions moves from the electrolyte to the metal/oxide boundary, which result in the growth of oxide at both sides (Thompson, 1997).

As the thickness increases, this will decrease the effect of electric field across the oxide hence limiting the growth capability of the oxide layer. Chung *et al* also concur that the outcome of the process leads to thickened of oxide barrier layer, forming a non-conductive barrier restricting the flow of ions. This results in the decrease of oxidation rate over time (Chung *et al.*, 2017).

The oxide electric field has a connection with the surface morphology of the aluminium alloy oxide templates. There is a tendency that electric field tends to concentrate more at the surface with morphology instability which will develop into pits shown in Fig. 2.3(b). Due to the parallel segment of the pits, the pit will enlarged into the shape of pores depict in Fig. 2.3(c) during oxide growth. This ripple effect will cause the pores to grow downwards until they fuse as shown in Fig. 2.3(d). Finally, anodic aluminium oxide template is formed at Fig. 2.3(d). The length of aluminium alloy oxide template increases linearly with the anodization time until the aluminium fully depletes (Thompson, 1997).

2.3.3 Synthesis Techniques of Anodic Aluminium Oxide Template

Surface modification process have been the most effective approach to improve the mechanical properties of Al alloys in different environments. Up to date, there are a number of published papers and reviews on the synthesis of nanostructures and its methods. Surface technology process for example anodization, physical vapor deposition, chemical vapor deposition, sol gel coatings and thermal sprayings serve as a feasible solution to widen the market share of aluminium alloys (Quazi, 2015).

Numerous research has been employed to address the corrosion, fatigue and tribological characteristics of AAO template without degrading the microstructure and modifying the composition. Throughout the years, various metal and oxides being researched and studied on, such as zinc oxide (ZnO) (Huang, et al., 2001), titanium oxide (Kasuga *et al.*, 1992) and others. The appropriate techniques are selected based on the application, layer thickness, and contact load.

Among all the fabrication methods used for the fabrication of Al₂O₃ template, anodization is by far the best approach for to fabricate oxide layer on the metallic surface.

2.3.3.1 Anodization

Anodization of aluminium and its alloys using sulfuric acid was patented back then in 1927's by Gower *et al* for corrosion protection and surface finishing (Kikuchi *et al.*, 2013). The factor affecting the thickness and quality of AAO is affected by the electrolyte concentration, temperature, current density, metal compositions and rate of anodization which will be discussed further.

Up to date, sulphuric acid is the most common acidic electrolyte for the formation of AAO as it forms barrier layer rather quickly and easily. AA6061 substrate fabricated by electrochemical anodization technique have gain popularity due to its highly ordered, well adherent AAO array. Table 2.1 below summarizes the anodization conditions employed previously by other researchers in the synthesis of AAO via different anodization technique including electrolyte composition, voltage, thickness and time

Table 2.1: Electrolyte composition coating on aluminium alloys

No	Electrolyte composition	Voltage (V)	Time (hours)	Ref.
1.	0.3 M H ₂ SO ₄ (Sulphuric Acid)	25	12.5	(Masuda & Hasegwa, 1997)
2.	0.3 M H ₂ C ₂ O ₄ (Oxalic Acid)	40	160	(Masuda & Fukuda, 1995)
3.	0.1 M H ₃ PO ₄ (Phosphoric Acid)	195	1	(Nielsch <i>et al.</i> , 2002)
4.	0.3 M H ₂ C ₂ O ₄ (Oxalic Acid)	30	1	(Chung <i>et al.</i> , 2010)
5.	1 M H ₂ SO ₄ + 1 wt. % HF	20	1	(Sieber <i>et al.</i> , 2005)
6.	0.3 M H ₂ SO ₄ (Sulphuric Acid)	15	1	(Ono, <i>et al.</i> , 2004)
7.	0.6 M H ₃ PO ₄ (Phosphoric Acid)	40	1	(Samantilleke, <i>et al.</i> , 2013)
8.	0.5M C ₄ H ₆ O ₅ (Malic Acid)	200	48	(Kikuchi, <i>et al.</i> , 2013)
9.	0.1 M H ₃ PO ₄ (Phosphoric Acid)	194	3	(Lee, <i>et al.</i> , 2011)

According to research being done, anodization is the most preferred process as it produces stronger surface adhesion, mechanical integrity such as strength and hardness, while providing good protective layer of the resulting implants (Sarhan, 2013). Consequently, anodization grown electrochemically on AA6061 was reported to increase the corrosion and wear resistance (Huang, *et al.*, 2001).

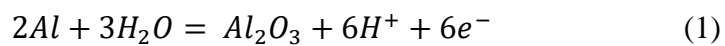
However, there are also drawbacks being reported solely to conventional anodization, which separates the corrosion and wear protection away from the substrate. This instance greatly affects the mechanical performance (Nayak, 2004). Evidence also showed that by using anodization in sulphuric acid solutions, this creates a porous close packed structure array with hexagonal cell making the structure highly absorbent, which allows the accumulation of unwanted material on solid surface to happen when exposed

to corrosive environments (Gonzalez *et al.*, 1999). In general, anodization changes the crystallographic and microscopic structure of metal surface, making it porous due to the thick coatings hence the requirement for sealing process (Grubbs, 1999).

2.4 Formation Mechanism of Alumina Nanoporous

Generally, the formation of AAO during anodization can be described as chemical dissolution followed by electrodeposition of anodic oxidation. In 1978, Thompson *et al* proposed a model to describe the two main process that took place during the initial film growth formation, which is the (i) growth by ionic migration through an existing film Al^{3+} , O^{2-} and OH^{-} forms new oxide layer near the aluminium film and (ii) dissolution between the electrolyte and aluminium oxide film at the interface level (Thompson *et al.*, 1978).

The geometric parameters of oxides layer are controlled by a set of process parameters such as the electrode properties, acid concentration, deposition time, anodization applied voltage and electrode separation distance. The formation of nanotubular pore arrays in aqueous based-solutions during electrochemical oxidation can be expressed by equation (1) and (2) below (Wu *et al.*, 2007). Equation (1) illustrates the oxide layer growth during anodization on the anode electrode.



The morphology features of anodic alumina pore growth can be divided into four stages as shown in Figure 2.4. During anodization, the immersed Al substrate will form a layer of barrier oxide on the entire surface area (Fig 2.4a). Due to external factors pertaining stress and defects, this leads to the formation of potential lines concentrated in a region, due to the development of penetration paths known as pore initiation (Fig 2.4b). The substrate is said to achieved pore development as it is an auto catalytic process (Fig 2.4c), and finally when it acheives steady state anodic film morphology occurring roughly at the same rate (Fig 2.4d) (Parkhutik & Shershulsky, 1992)

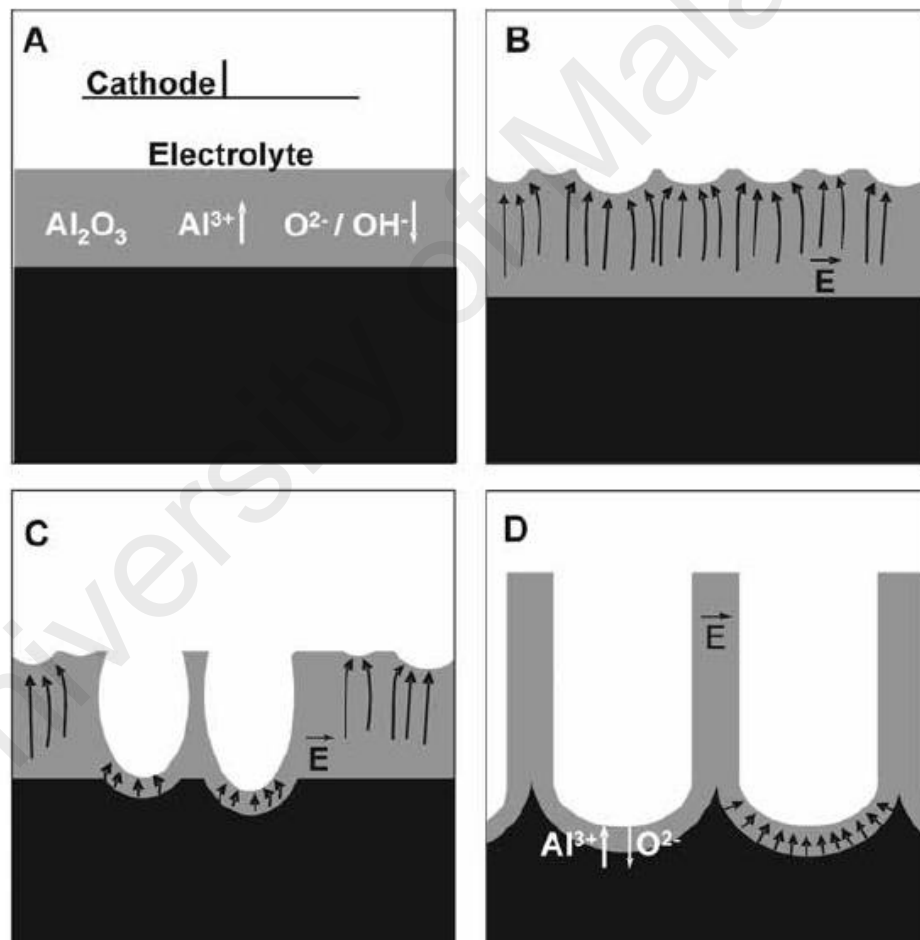


Figure 2.4: Growth formation of porous AAO (Parkhutik & Shershulsky, 1992)

2.5 Processing Parameters Effects on the Development of Porous Alumina

The research done by Masuda and Fukuda in 1995 has garnered much attention in the generation of anodic porous alumina oxide. Example of the structure is showed in Figure 2.5. Numerous studies were conducted to grow a perfectly close packed hexagonal anodic porous alumina, varying from the right electrolyte concentrations and temperatures, voltages, pre-treatment and purity of the initial Al substrate.

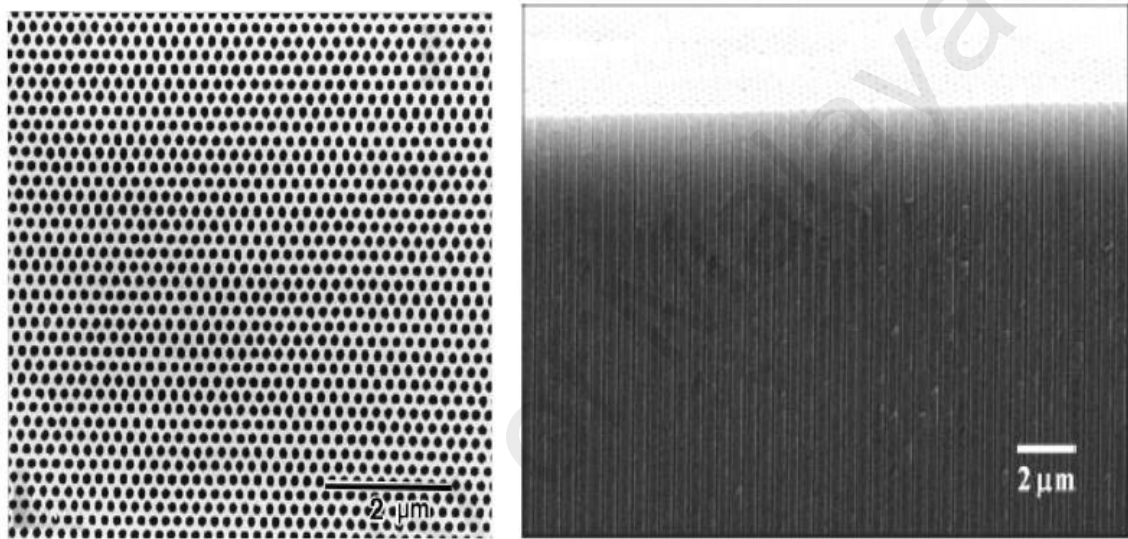


Figure 2.5: SEM view (left) and cross-sectional view (right) of perfect hexagonal anodic porous alumina oxide layer (Masuda, *et al.*, 2001).

2.5.1 Effects of Anodization Voltage to the Formation of Anodic Aluminium Oxide

Lately, Ono *et al.* proposed that the factor for obtaining a self-porous alumina oxide depends on the current density during film growth. It was noted that the homogeneity of cell size improves in tandem with increased of potential voltage followed by the rise in current density (Ono *et al.*, 2004). Bandyopadhyay *et al.* reviewed that electropolishing of aluminium at high current density may formed pits. By anodizing this electropolish aluminium will result in a perfect hexagonal porous order arrangement (Bandyopadhyay, *et al.*, 1996).

The interpore distance of porous oxide formed during anodization increases with the anodizing voltage (Chu, *et al.*, 2006). Thus, the higher the anodizing voltage employed during anodization, the larger the interpore distance also known as interpore distance. The formation of hexagonal pore array also depends on the voltage applied (Jessensky *et al.*, 1998).

2.5.2 Effects of Anodization Surface on the Formation of Anodic Aluminium Oxide

Pre-treatment of Al substrate also played a part in the equipotential strength of the model as the preferred pore growth direction should be perpendicular to the surface of oxide layer. It is believed that a coarser surface may affect the pores alignment making it not parallel to each other whereby affecting the electric field strength (Su & Zhou, 2009). It has been found that only certain anodization conditions will initiate self-organization of the pores. The term self-organized is coined when the nearest neighbor pore and lattice is arranged hexagonally according to the radial distribution function and was reported to exhibit photonic crystal properties (Choi *et al.*, 2003).

2.5.3 Effects of Anodization Electrolyte to the Formation of Anodic Aluminium Oxide

It was reported that the types of electrolyte composition used can influence the change in surface properties. These include the strength and hardness of substrate, microstructure, morphology and tribological properties. A variety of acidic acids are carried out whereby the cathode and anode are immersed in several distinct electrolytes such as sulphuric acid (Cheng & Chou, 2015), oxalic acid (Chen *et al.*, 2010; Wang *et al.*, 2008) and phosphoric acid (Masuda *et al.*, 1998; Zhang *et al.*, 2010). The thickness

of the film growth is also determined by the directionality of the electrolyte (Wood *et al.*, 1996).

The mixture of electrolyte type was also reported useful to control the anodizing voltage and cell pores diameter. Several mixture groups such as sulphuric acid/oxalic acids (Shingubara *et al.*, 2004; Kashi *et al.*, 2007) and oxalic/phosphoric acid (Kao & Chang, 2014) were performed for the anodic aluminium oxide formation.

2.6 Other Anodic Metal Oxides

Anodization, grown electrochemically on aluminium alloy have been studied extensively by numerous researchers to produce porous oxides matrix aside from the common metals. To date, not only aluminium materials are widely researched on to produce porous oxide films, but rather a variety of other metals. Among the metals research are niobium (Nb)(Tsuchiya *et al.*, 2005), titanium (Ti)(Beranek *et al.*, 2003), tungsten (W) (Mozalev *et al.*, 2016), tantalum (Ta) (Young, 1960), and zirconium (Zr) (Cox *et al.*, 1970).

2.6.1 Anodization of Niobium

Studies have showed that Nb nanotubes by anodization have desirable application properties as gas sensors, optical, catalysts and electrochromic devices. Self-organised porous hafnium were first obtained via anodization in 1 M H₂SO₄ + 0.2 wt% NaF with constant potential of 50 V at atmospheric temperature depicted in Figure 2.6 (Tsuchiya & Schmuki, Self-Organized High Aspect Ratio Porous Hafnium Oxide prepared by Electrochemical Anodization, 2005). On another note, highly ordered porous niobium oxide (Nb₂O₅) films were performed in 1M H₂SO₄ with addition of 1% HF respectively

(Sieber *et al.*, 2005). Based on the research, the potential anodization voltage was found to be the leading key affecting the microstructure of AAO and its morphology.

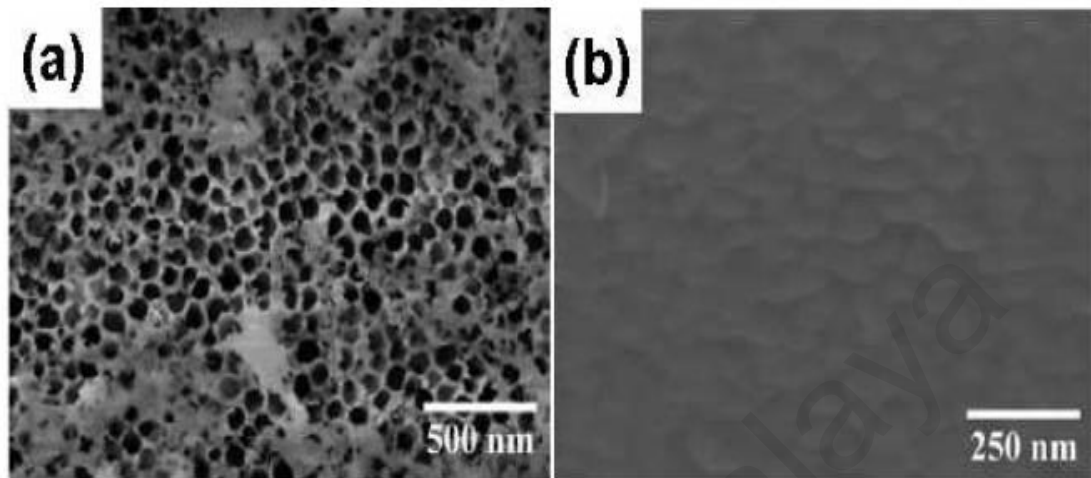


Figure 2.6: Porous Nb₂O₅ (a) view and (b) side view anodized in 1 M H₂SO₄ + 0.2 wt% NaF (Tsuchiya & Schmuki, 2005).

2.6.2 Anodization of Tungsten

Tungsten oxide, (WO₃) gained its popularity due to its commercial and potential application in photocatalytic, optical data storage device, and solar cells. Electrochemical anodization of tungsten was investigated in 0.2 M H₃PO₄ aqueous solution. With the current technology in this approach, the anodic WO₃ films growth with nanoporous layer forming a homogenous anodic film (Mozalev *et al.*, 2016). Apart from that, porous anodic WO₃ showed denser pores with small size distribution in the morphology structure when anodized in 0.3 M oxalic acid, (H₂C₂O₄) as represented Figure 2.7 (Tacconi, et al., 2006).

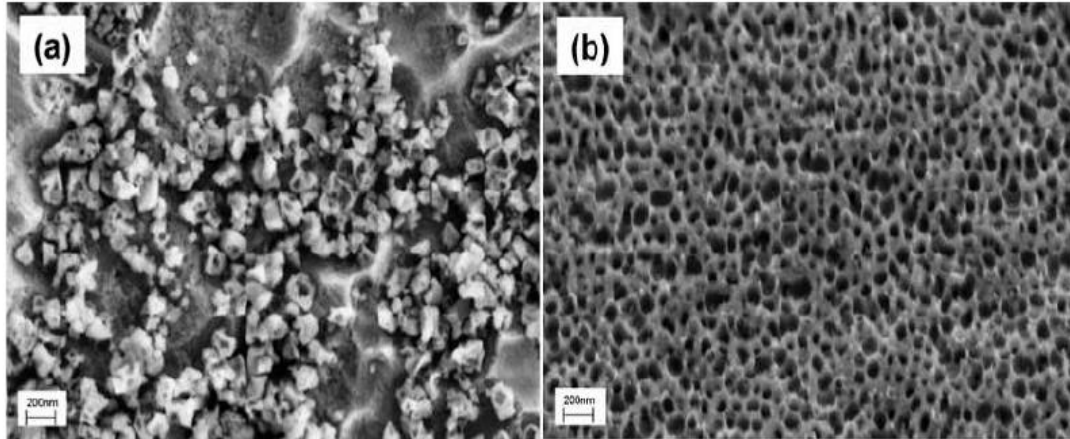


Figure 2.7: Porous WO_3 (a) view and (b) side view anodized in 0.3 M $\text{H}_2\text{C}_2\text{O}_4$ at (a) 10 V, (b) 35 v. (Tacconi, et al., 2006)

2.6.3 Anodization of Titanium

Research in titanium oxide, (TiO_2) have attracted multiple attention due to its high potential in self-cleaning materials, gas-sensors, photovoltaics and photoanode solar cells. Self organized porous TiO_2 layers were obtained using 1 M H_2SO_4 at room temperature. Beranek and co-workers anodized titanium metal in H_2SO_4 electrolytes containing low concentration of HF (0.05-0.4wt %). As a result, the optimized electrolyte produced a highly ordered porous TiO_2 , comprised of single pore arrays with pore spacing of 150 nm and an average diameter of 140 nm (Beranek *et al.*, 2003). Apart from that, Mor et al reported that addition of acetic acid to HF electrolyte results in a more robust nanotubes without altering its size and shape (Mor *et al.*, 2003).

2.6.4 Anodization of Zirconium

Zirconium oxide, (ZrO_2) is used as a catalysts support and industrial catalyst. The electrochemical formation of ZrO_2 in 1 M H_2SO_4 + 0.2 wt% NH_4F with constant potential of 30 V results in the growth of porous ZrO_2 layers as presented in Figure 2.8. The growth of ZrO_2 layer leads to the transition of amorphous to crystalline film at room temperature

(Tsuchiya *et al.*, 2005). It was reported that ZrO_2 layer is able to form up to several hundreds of nanometers even if culturally anodized in various forming electrolytes (Cox, 1970).

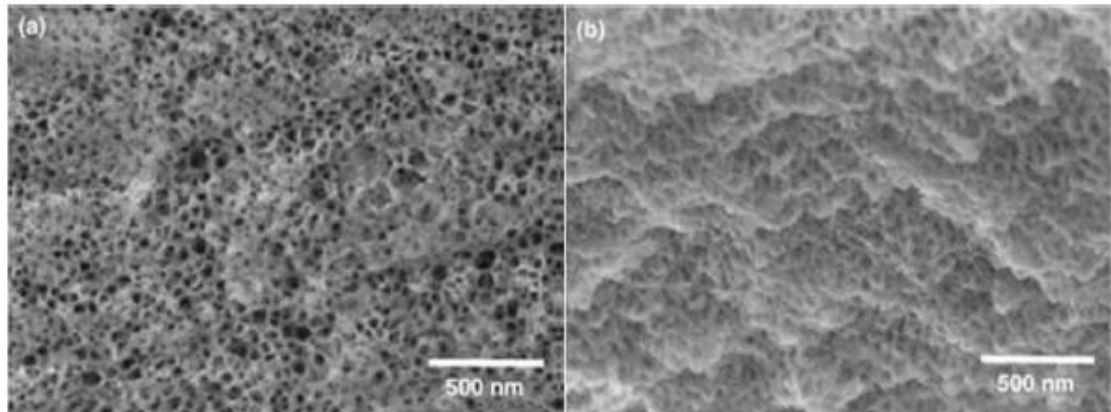


Figure 2.8: Porous ZrO_2 (a) view and (b) side view anodized in 1 M H_2SO_4 + 0.2 wt% NH_4F electrolyte at 30 V. (Tsuchiya & Schmuki, 2005).

2.6.5 Anodization of Tantalum

Tantalum oxide, (Ta_2O_5) has been regarded as a protective coating material for equipment. Anodization of tantalum was successfully investigated in various acidic and neutral electrolytes such as phosphoric, sulphuric acid, and sodium sulfate solution (Young, 1960). The result produced a layer of amorphous Ta_2O_5 with constant thickness as shown in Figure 2.9. Self-organized porous Ta_2O_5 was successfully obtained in 1 M H_2SO_4 with constant potential of 20 V (Sieber *et al.*, 2005).

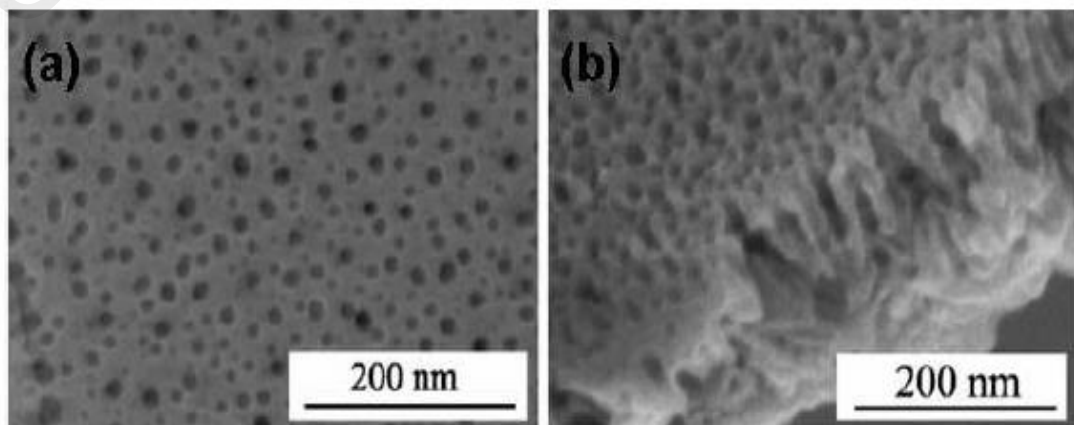


Figure 2.9: SEM image of porous Ta₂O₅ (a) view and (b) side view anodized in 1 M H₂SO₄ electrolyte at 20 V (Sieber *et al.*, 2005)

2.7 Two-Step Anodization of Aluminium

To reiterate, it was only in 1995 that Masuda and Fukuda discovered the formation of AAO with highly ordered nano-pores. The pores were reported to aligned regularly forming a honeycomb structure and this have encouraged researchers to further research on the development of “two-step anodization”.

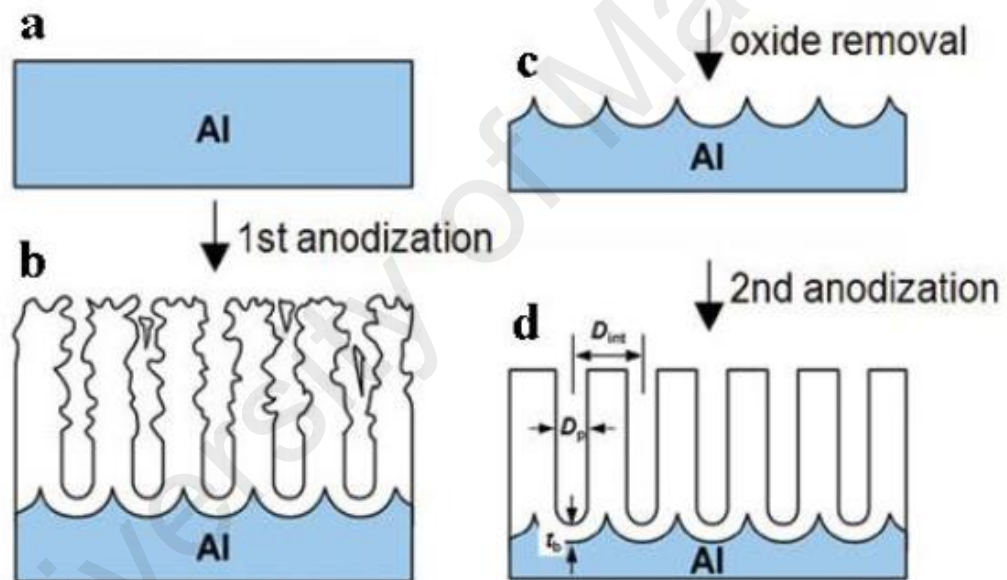


Figure 2.10: Schematic of two-step anodization process involving, (a) electropolished surface, (b) first anodization, (c) oxide removal and (d) second anodization (Zaraska *et al.*, 2010)

First and foremost, Al substrates are electropolished under constant voltage in acidic solution. During the first anodization step in (Fig 2.10b), the electropolished Al substrate is anodized in acid electrolyte. As observed, no well-ordered hexagonal pores arrangement is formed. Pores start to grow downwards towards aluminium base until all the tube bottom are parallel to each other. Subsequently, oxide is removed by submerging

the initial-anodized substrate templates in H_2SO_4 (Zaraska *et al.*, 2010). By removing the oxide in (Fig 2.10c), a pit is formed in the aluminium surface. Finally, the AAO template is anodized for the second time shown in (Fig 2.10d) to produce a surface consisting of symmetrical nanopores with acquired pore diameter and thickness (Zhao *et al.*, 2007; Lee *et al.*, 2011). A research conducted by Ilango *et al* also noticed the similar formation of self organised nanoporous on Al substrate (Ilango *et al.*, 2016)

2.7.1 Hardness of Al and Al_2O_3 Nanoporous

Hardness of a material is determined by Vickers hardness number. An experiment conducted by researchers on Al_2O_3 with different alloy composites AA356 and AA1050 sintered at 1200 °C returned with hardness value of 610 HV and 153 HV, respectively. This proved that the higher content of Al alloy in the composite is known to affect the hardness of pure alumina as aluminium is comparably a soft material. According to Chou *et al.*, the hardness properties value of aluminium and Al_2O_3 depends on the number of pores in the composites (Chou *et al.*, 2007). This is due to the voids found which influenced the physical and mechanical properties of the composites. Therefore, the composition of Al in A356 was bigger than Al A1050 based on the vickers hardness value side. The formation of pores also relied on densification of pore formation in the microstructure. A research proved that the increase of Al_2O_3 lamination thickness lowers the hardness value of the metal due to the increase of porosity and coating roughness (Sarikaya, 2005). This causes the lamination to be mechanically weakened with the increase in pores and residual stresses. In fact, the increase in hardness can be obtained at a lower coating thickness with lower porosity and surface roughness.

2.7.2 Wettability of Al and Al₂O₃ Nanoporous

The wettability of nanoporous Al₂O₃ were investigated by the water contact angle. Tuscharoen et al reported an increase in surface contact angle from 38° to 106° by increasing the anodization voltage which changes the surface properties from hydrophilic to hydrophobic. It showed that the increase in anodization voltage affects the template morphology (Tuscharoen, et al., 2017). The convention term of superhydrophobic (WCA over 150 °) were made known in recent years which attracted research interest due to its promising application in microfluidics and self-cleaning surface (Barberoglou *et al.*, 2010; Buijnsters *et al.*, 2013) Aside from that, a similar trend on super-hydrophobic with high contact angle can also be achieved by surface modification via plasma enhanced chemical vapor deposition (PECVD) (Tuscharoen, et al., 2017).

2.7.3 Corrosion of Al and Al₂O₃ Nanoporous

Different grades of aluminium react differently in contact with various types of acids. Hence, corrosion of Al materials is examined for a few reasons. A research reported that the dissolution of grain boundary is dependent on the corrosive effects of acids (Schacht *et al.*, 2000). It is, therefore, believed that the corrosive effect on alumina increases in the acids order H₂SO₄ > HCl > H₃PO₄ (Curkovic *et al.*, 2008). On top of that, Curkovic et al., in their alumina corrosion tests recorded that the dissolution rely on the grain boundary impurities (Curkovic & Jelaca, 2009). Hence, this proved that impurities played a role in the corrosion process of alumina and its alloys.

2.8 Heat treatment of Al and Al₂O₃ Nanoporous

Various steps are introduced to produce a highly ordered hexagonal porous structure, but little work has been investigated on the influence of heat treatment. Different conditions were proposed by researchers on the heat treatment. In 2007, a

research on heat treatment in nitrogen atmosphere at 500 °C for 4 h were done to obtain homogenous microstructure and to enlarge the grain size (Zhao, *et al.*, 2007). Annealing process is reported to softens the aluminium as several dislocation moved into lower-energy configurations producing a new strain-free grains (Rahimi *et al.*, 2008). It is also studied that annealing along with electropolished treatment improved the oxide stability against dissolution which could be an indication of uneven distributions of oxide (Bocchetta *et al.*, 2003). According to Vatne *et al.*, annealing at 620 °C for 24 h proved that heat treatment has a profound influence on the final grain size and recrystallisation texture (Vatne *et al.*, 1994). At lower annealing temperature, the grain size decreases in tandem with temperature. Aside from that, the effect of higher annealing temperature also leads to improved microhardness value and reduce porosity as the thicker coating layer is mechanically weakened with increasing pores and residual stresses (Sarikaya, 2005).

CHAPTER 3: MATERIALS, METHODS AND PROCEDURES

Chapter 3 reviews the methodology process to fabricate nanoporous anodic alumina on aluminium alloy series 6 substrates via electrochemical anodization along with the materials, equipment, and experimental settings involved in this project as well as its characterization for mechanical and tribo-corrosion properties. Figure 3.1 shows the flowchart process

University of Malaya

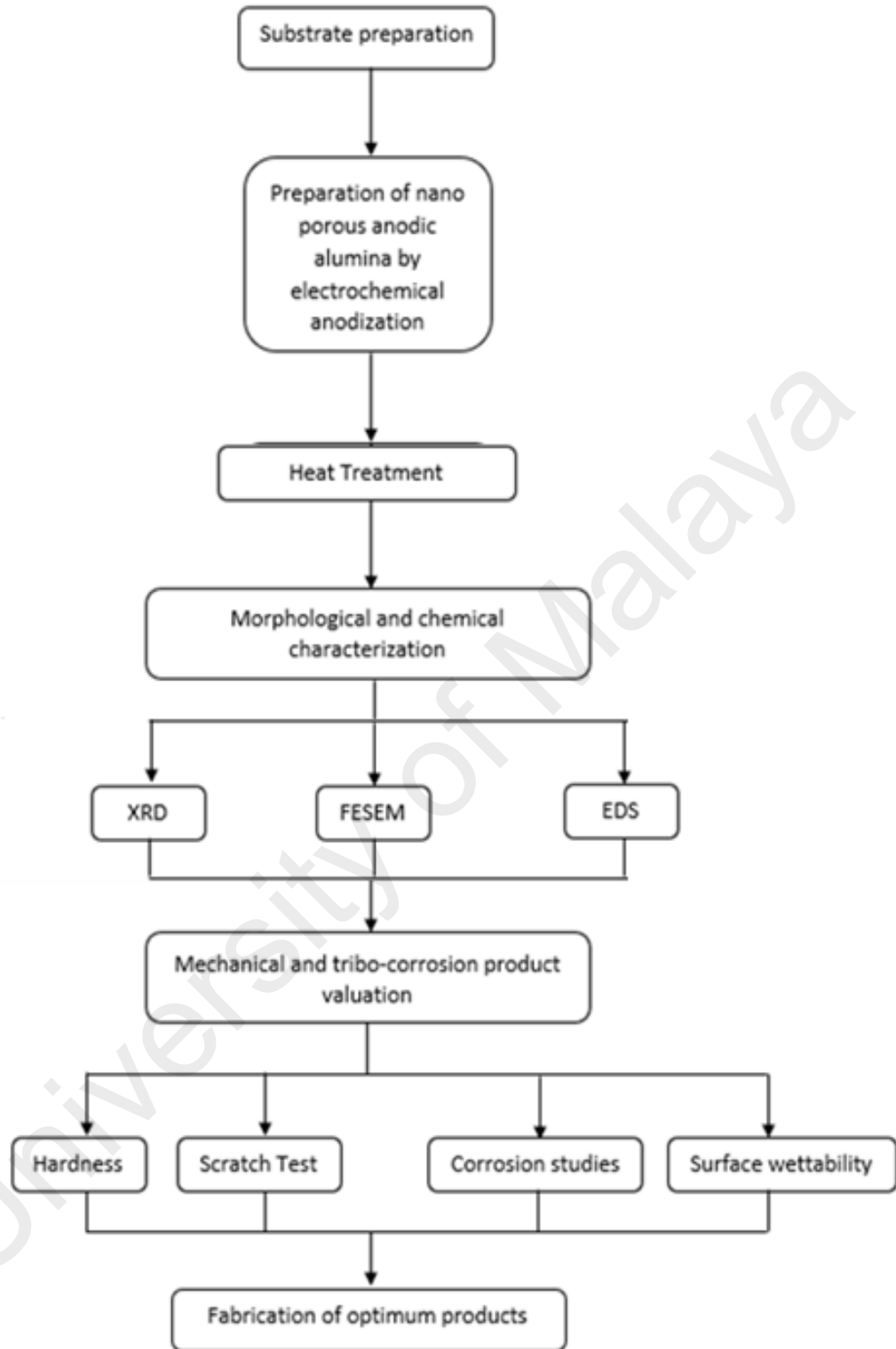


Figure 3.1: Schematic diagram of nanoporous anodic alumina on AA6061 metal

3.1 Substrate Preparation

The raw material used in this study was fabricated from aluminium alloy series 6 (KAMCO ALUMINIUM SDN BHD, Kuala Lumpur, Malaysia) metal. The substrate was cut into thin plates with dimensions of 15 mm × 15 mm × 2 mm.

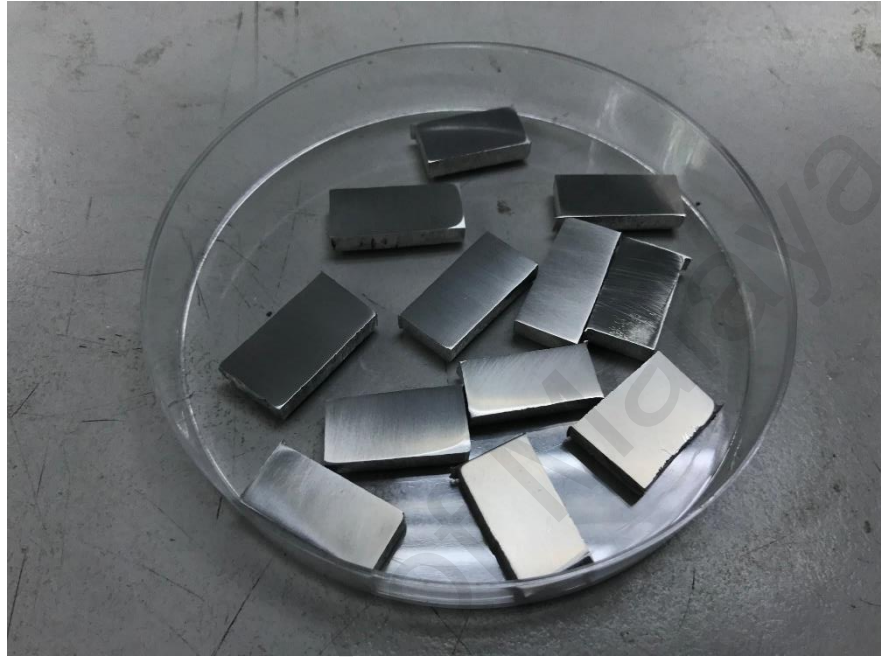


Figure 3.2: AA6061 T657 plates after cutting into smaller plates

Following that, the specimens were successfully abraded (Model METAPOL-2, Srimad) using emery paper with different grit ranging from 800-2400, for 1 minute both each in Figure 3.3, followed by wet-polishing using diamond slurry to mirror finish. The default speed for both grinding and polishing are set at 500 rpm.

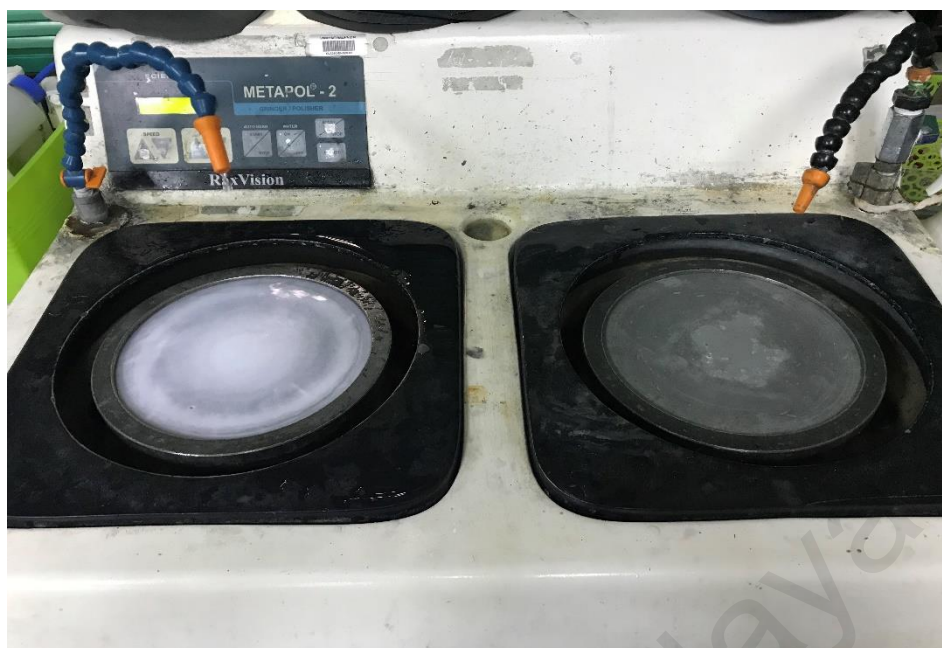


Figure 3.3: Grinder and polisher machine (Model METAPOL–2, Srimad).

Samples were placed in an ultrasonic cleaning bath dipped in acetone at a temperature of 40 °C for 10 minutes. The substrates are then washed with distilled water, followed by drying for each individual sample in order to fabricate Al₂O₃ nanoporous array.

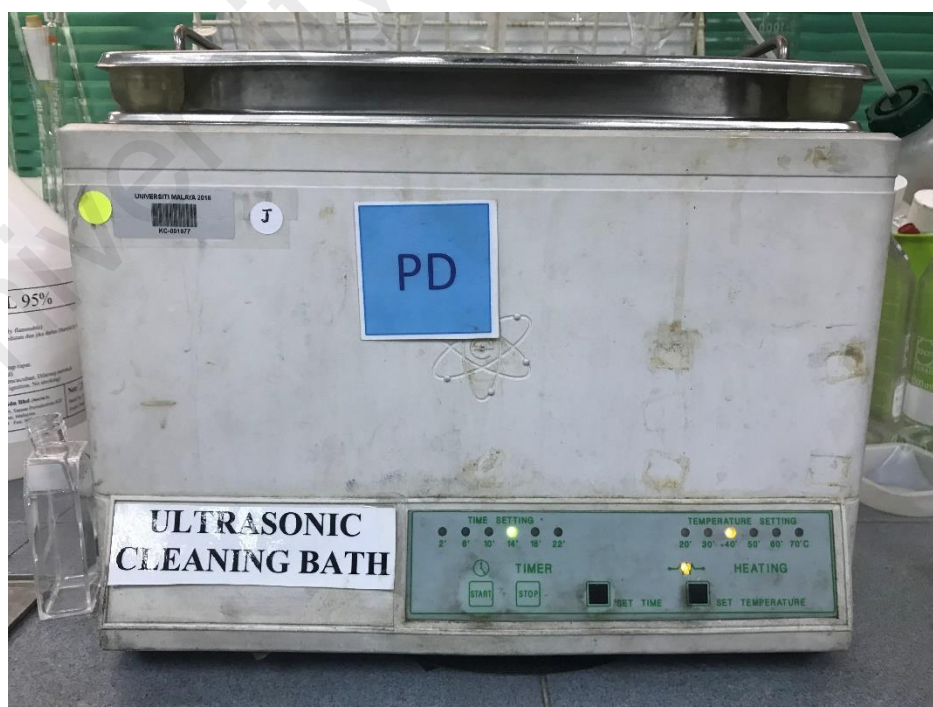


Figure 3.4: Ultrasonic cleaning bath

3.2 Preparation of Self-Organized Al₂O₃ Nanoporous Arrays

Anodization of substrate AA6061 T657 was conducted in an electrochemical cell consist of two-electrode by using a direct current (DC) power source (Model E3641A, Agilent Technologies, Palo Alto, USA) rated at 12V for 1 hour in sulfuric acid (15 wt% H₂SO₄, Ajax Chemicals, Sydney, Australia). It is important that the electrodes and graphite rod are cleaned and polished before used to prevent surface impurities which might affect the adherence and strength of deposition. The graphite rod (D = 5mm) was connected to the negative terminal (cathode) and the samples were connected to the positive terminal (anode) of the power supply (Model EPS 601, General Electric) at room temperature. The distance between the anode and cathode terminal are separated 20 mm away in all experiments. Subsequently, samples are then rinsed with de-ionized water to remove residual and impurities from the surface. The setup of electrochemical anodization is shown in Figure 3.5.

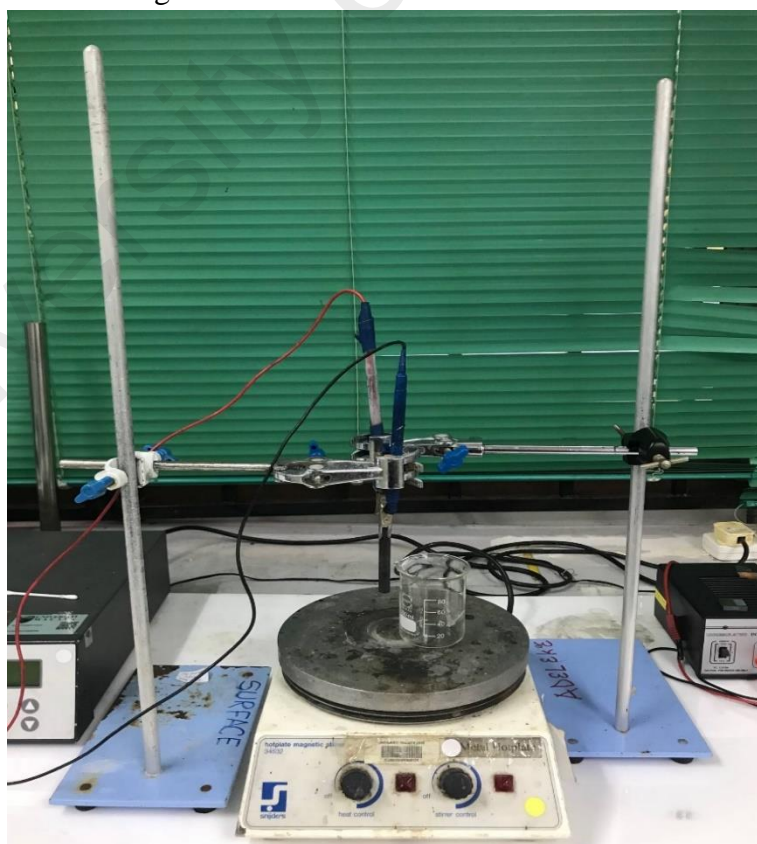


Figure 3.5: Electrochemical anodization process to produce Al₂O₃ nanoporous array

3.3 Annealing

Subsequently, to improve the coating adhesion, heat treatment was carried out. The amorphous coated sample undergoes annealing in a standard laboratory furnace. For the samples to form crystalline phases, the anodized specimens were heat treated at ambient temperature up to 450 °C for 1.5 h, pre-set at an increase and decrease temperature elevation ramp of 5 °C/min under atmospheric conditions. Samples were placed in the middle of the furnace for even heat distribution.



Figure 3.6: Furnace for annealing of substrate

3.4 Characterization Techniques

A variety of characterization techniques were employed in this work to analyze the AAO template formation after undergoing all processes. The analytical methods used are field emission scanning electron microscope (FE-SEM), X-ray diffraction (XRD), energy dispersive x-ray spectroscopy (EDS) and atomic force microscopy (AFM).

3.4.1 Field Emission Scanning Electron Microscope

In this present work, morphology of coating was investigated by using (FESEM, SU8000, Hitachi, Japan) with an acceleration voltage of 1 to 2kV.

3.4.2 X-Ray Diffractometry

XRD is a technique used to characterize crystalline materials. In short, it acquires information based on the current phase, crystallographic structures and chemical composition of coated AAO template.

In this present work, the phase composition and purity of the substrates, Al₂O₃ nano porous arrays on series 6 specimens were analyzed by (XRD, PANalytical X'Pert 3 Powder, Netherlands) with Cu K α radiation ($\lambda=1.54178 \text{ \AA}$) operating at 45 kV and 30 mA, 2θ range of 20° - 80°, scan rate of 0.1°·s⁻¹, and step size of 0.026°. The "PANalytical X'Pert HighScore" software was employed to determine XRD patterns, whereby patterns are governed by the standards gathered by the Joint Committee on Powder Diffraction and Standards (JCPDS, card #005-0682).

3.4.3 Energy Dispersive X-Ray Spectroscopy

EDS or otherwise known as EDX are one of the many analytical technique used to analyze and obtain compositional analysis. Hence, the atomic concentration are respectively determined using EDS.

3.5 Adhesion Strength

The lamination strength of the coating was measured using Micro Materials Nano Test (Wrexham, United Kingdom) equipped with a diamond indenter. The angle of the indenter was set at $90.0 \pm 5.0^\circ$ and tip radius of $25 \pm 2.0 \mu\text{m}$. The experiments were performed with a loading rate gradually increased to 9.2 mN s^{-1} and a sliding velocity of 5 mm s^{-1} . The scratch tests were performed on each individual sample. Samples are moved in a perpendicular manner towards the scratch probe while the contact are held constant. Subsequently, the result based on the scratch profile were examined under an optical microscope (Olympus BX61, Tokyo, Japan). The frictional load and probe penetration depth were monitored throughout the test to determine the critical normal force required to peel of the oxide layer coatings off the substrate. Each sample was scratch tested for three times under the same parameter to ensure reproducibility of the results.

To investigate further, the scratch hardness test was performed on the substrate, Al_2O_3 nanoporous array, and heat treated Al_2O_3 nanoporous array thin film at 450°C for 1.5 hours. The purpose of the test performed is to measure the lamination of oxide of the single point force exerted which caused the deformation. Once completed, the stylus tip is removed to compute the scratch hardness which can be calculated by dividing the applied normal force exerted by the stylus tip against the final scratch width. Based on that, the frictional coefficient can also be obtained at the critical load by the tester. The

scratch hardness number, HS_P is determined using the following specification of ASTM G171-03 governed by the formula below (ASTM, 2003; Jaworski *et al.*; 2008);

$$HS_P = \frac{8P}{\pi w^2} \quad \text{Eq. (1)}$$

Where HS_P is the scratch hardness number, P is the applied normal force, and ‘ w ’ is the scratch width.

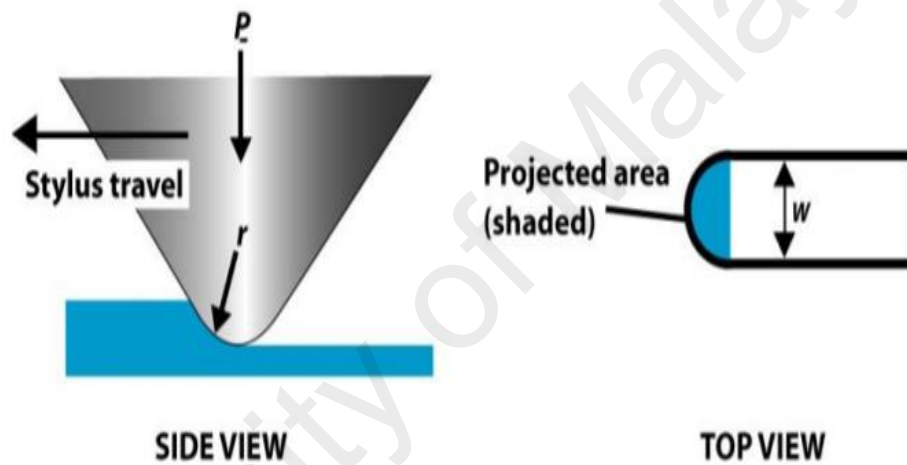


Figure 3.7: Schematic of scratch hardness measurement (Li D. J., 2009)

3.6 Microhardness

The Vickers microhardness testing machine (Mitutoyo-AVK C200-Akashi Corporation, Kanagawa, Japan) was employed to determine the microhardness of each samples by the strength-indentation method with an applied load of 98.07 mN and dwell time of 15 s at ambient temperature. A total of five indentations was analyzed to determine the average mechanical properties of each.

3.7 Corrosion Studies

Corrosion specimens were analyzed using potentiostats/galvanostats (SP-150, Bio-Logic, France). The potentiodynamic polarization was executed using a three electrodes terminal in a compartment cell: (i) a sample as the working electrode, (ii) a counter electrode made of platinum, and (iii) the saturated calomel electrode as the reference electrode. All samples were performed in an artificial seawater. The substrate, AAO, and heat-treated samples were the working electrodes exposed using a mounted sample with working area of 1 cm².

Potentiostat SP-150 was monitored by a PC computer and EC-Lab software were used to collect and evaluate the experimental data. The potential range varying from -2000 to +2000 mV were tabulated in the polarization curve against reference electrode with a scanning rate of 1 mVs⁻¹. Duplicate tests were performed under identical testing conditions to validate reproducibility.

As mentioned, the corrosion study was performed in artificial seawater by dissolving inorganic salts at stagnant room temperature. As reported by Burkhoder's formulation, the compositions of the simulated seawater were as follows (per litre of deionized water);

23.476 g NaCl + 3.917 g Na₂SO₄ + 0.192 g NaHCO₃ + 0.664 g KCl + 0.096 g KBr + 10.61 g MgCl₂ · 6H₂O + 0.026 g H₃BO₃ + 0.04 g SrCl₂ · 6H₂O + 0.41 g MgSO₄ · 7H₂O + 0.1 g NH₄Cl + 0.1 g CaSO₄ + 0.05g K₂HPO₄ + 0.5 g tri-sodium citrate + 3.5 g sodium lactate + 1 g yeast extract (Bidwell & Spotte, 1985). The pH was adjusted to 7.5 ± 0.1 using 5 M NaOH solution (Yuan *et al.*, 2013).

The corrosion potential (E_{corr} / V_{SCE}), and corrosion current ($I_{corr} / \mu A \text{ cm}^{-2}$), are obtained from Tafel graph. The corrosion protection efficiency ($P.E$) used to evaluate the effectiveness of corrosion protection was estimated governed by equation below (Yu *et al.*, 2014);

$$P.E.(%) = \frac{I_{corr}^0 - I_{corr}^c}{I_{corr}^0} \times 100 \quad \text{Eq.(2)}$$

Where I_{Corr}^0 is the corrosion current ($\mu A / \text{cm}^2$) of AA series 6 and I_{Corr}^c is the corrosion current of the coated samples.

CR was calculated by the following formula:

$$CR(mm\text{year}^{-1}) = \frac{0.13I_{corr} (E.W.)}{d} \quad \text{Eq.(3)}$$

3.8 Surface Wettability

The surface wettability (hydrophilicity) of nanoporous anodic Al_2O_3 was analyzed by measuring the contact angles of sessile drops of artificial sea water with a constant liquid volume of $5\mu l$ deposited on each sample surface for contact point assessments, with a drop speed of $2\mu l \text{ s}^{-1}$ at a temperature of $26 \pm 1 \text{ }^\circ\text{C}$. The webcam (OCA 15EC, Data Physics Instrument GmbH, Germany) was aligned to the eyepiece of microscope to study the surface wettability. The contact angle ' θ ' was measured by the water droplet height ' h ' and width ' w ' governed by the following formula (Elias *et al.*, 2008);

$$\theta(^{\circ}) = 2 \tan^{-1} \left(\frac{2h}{d} \right) \quad \text{Eq.(4)}$$

Wettability of surface contact angle can be viewed by the following (Rodrigues, 2017);

$$\left\{ \begin{array}{ll} \theta_{\infty} \approx 0^{\circ} & \text{superhydrophilic,} \\ 0^{\circ} < \theta_{\infty} < 65^{\circ} & \text{hydrophilic,} \\ 65^{\circ} < \theta_{\infty} < 150^{\circ} & \text{hydrophobic,} \\ \theta_{\infty} > 150^{\circ} & \text{superhydrophobic} \end{array} \right.$$

University of Malaya

CHAPTER 4: RESULTS AND DISCUSSION

4.1 XRD Analysis

Figure 4.1 shows the XRD profiles of the substrates (AA6061 T765), the 1 h anodized sample in H₂SO₄ solution with a constant potential of 12 V, and the heat-treated sample at 450 °C for 1.5 h (at heating and cooling rate of 5 °C / min). As depicted in Figure 4.1a, the XRD reflection of the substrate shows multiple diffraction peaks associated with Al located at $2\theta = 38.5^\circ$, 44.6° , 64.9° , and 78.1° , which are connected to the (1 1 1), (2 0 0), (2 2 0) and (3 1 1) lattice planes respectively. Subsequently, the 1 h anodized sample was formed as depicted in Figure 4.1b. After anodization, as can be seen, the intensity of characteristic peaks of Al especially (2 2 0) and (3 1 1) decreased which can be caused by the formation of oxide layer during the anodization. New diffraction peaks (1 1 1) plane were recorded at $2\theta = 38.3^\circ$, (2 0 0) plane at $2\theta = 44.6^\circ$, (2 2 0) plane at $2\theta = 64.5^\circ$ and (3 1 1) plane at $2\theta = 78.4^\circ$ individually. During annealing at 450 °C as shown in Figure 4.1c, same diffraction peaks (1 1 1) plane at $2\theta = 38.4^\circ$, and (2 0 0) plane at $2\theta = 44.6^\circ$ were recorded. It is noticeable that the intensity of the peaks increased considerably before and after annealing indicating their transition from amorphous to crystalline phase, as shown in Fig 4.1b and Fig 4.1c. The increased in the intensity of the peaks along with increase annealing temperature was also reported by Rao (Rao *et al.*, 2013). Aside from that, the decreased in the intensity of the Al peaks especially for (1 1 1) plane and the disappearance of (2 2 0) and (3 1 1) peaks contributed to the development of oxide layer formed on the surface of Al. However, due to amorphous and low crystalline nature of ceramic materials, the peaks identification of alumina is difficult to decipher. Grain size was reported to become larger during heat treatment, since grain coarsening and recrystallization occurs during annealing (Xu, et al., 2010). According to De Azevedo *et al.*, the broad peak indicates that the synthesized layer was disordered and/or made up of amorphous Al oxide compound (De Azevedo *et al.*, 2004). It is clear that there is high and sharp diffraction peak in these patterns, demonstrating that the Al₂O₃ coating phase is crystalline.

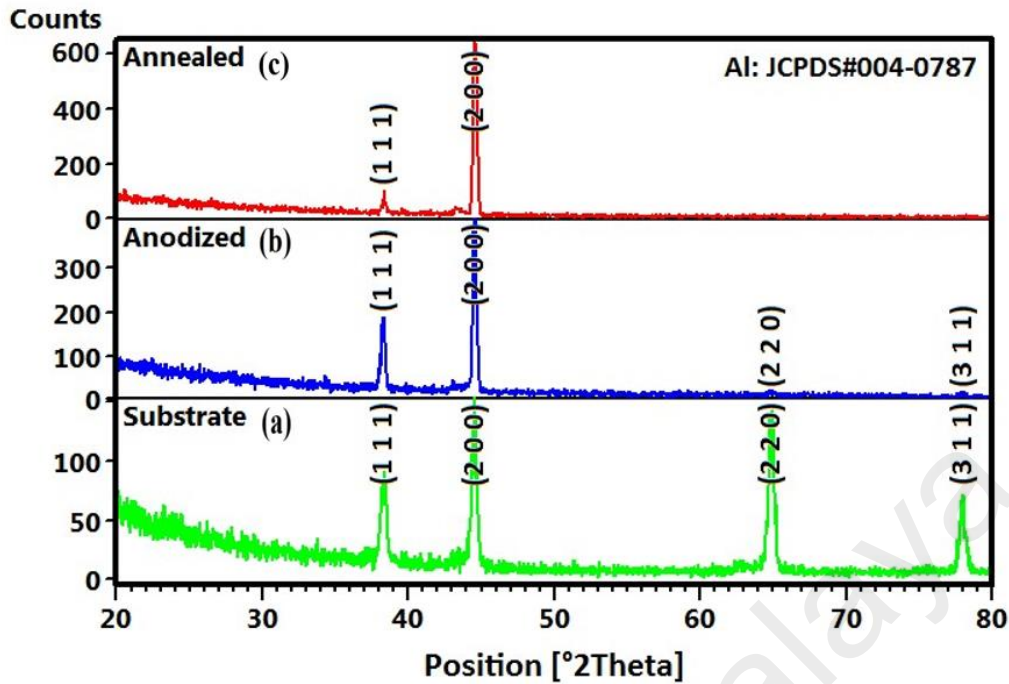


Figure 4.1: XRD profiles of the (a) bare substrate, (b) the anodized sample, and (c) the heat treated sample at 450 °C for 1.5 h

4.2 Microstructure of Al₂O₃ Nanoporous Array after Anodization

The microstructural evolution and chemical compositional analysis of AA6061 substrate and anodized specimens were observed by FESEM and EDS imaging technique individually at a time. The oxide coating was produced by anodizing aluminium substrate in 15 wt% H₂SO₄ electrolyte with a constant potential of 12 V for 1 h.

Microscopic examination was done to verify the effect of anodization as compared with the standard substrate specimen. As shown in Figure 4.2a, it is noticeable that the scratches, particles and organic contaminants are present based on the roughness of the surface, which could be due to the manufacturing process. Research performed by Runge in 1999 reported that defects such as grain boundaries, and surface contamination will affect the passivation of oxidation reaction (Runge J. , 1999). A comparative FESEM image in Figure 4.2a and 4.3a showed that the anodization process affects the surface

topography resulted in irregular formation of pits at the surface due to localized dissolution of the oxide layer.

Figure 4.2b shows the overall AA6061 substrate composition. The EDX analysis for the substrate recorded peaks for the primary alloying elements of aluminium at 92.54 wt%, followed by oxygen at 5.85 wt%, magnesium of 0.88 wt% and 0.74% wt% of silicon. The trace of oxygen is due to the formation of native oxide layer on the surface upon exposure to atmospheric air (Rulik, 2014). It should be noted that certain trace quantities of chemical elements are not detected during EDX analysis.

Figure 4.3b demonstrates the EDX spectra of coating of Al₂O₃ nanoporous array after anodized in 15 %wt H₂SO₄ for 1 h at a constant potential of 12 V. Results showed that aluminium and oxygen are the main elements of the coating formed in AAO after anodization from the EDX profile, which shows the formation of film layer on the substrate. From there, the profile also exhibit the absence of impurity during the anodization process.

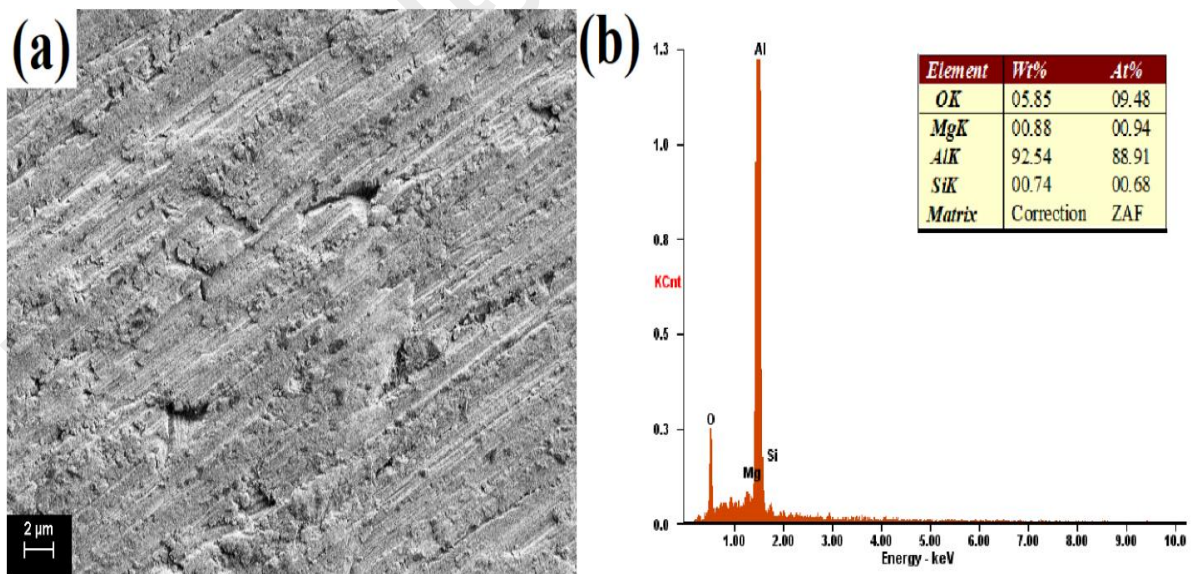


Figure 4.2: (a) Top view FESEM image and (b) EDX analysis of AA6061 series 6 substrate

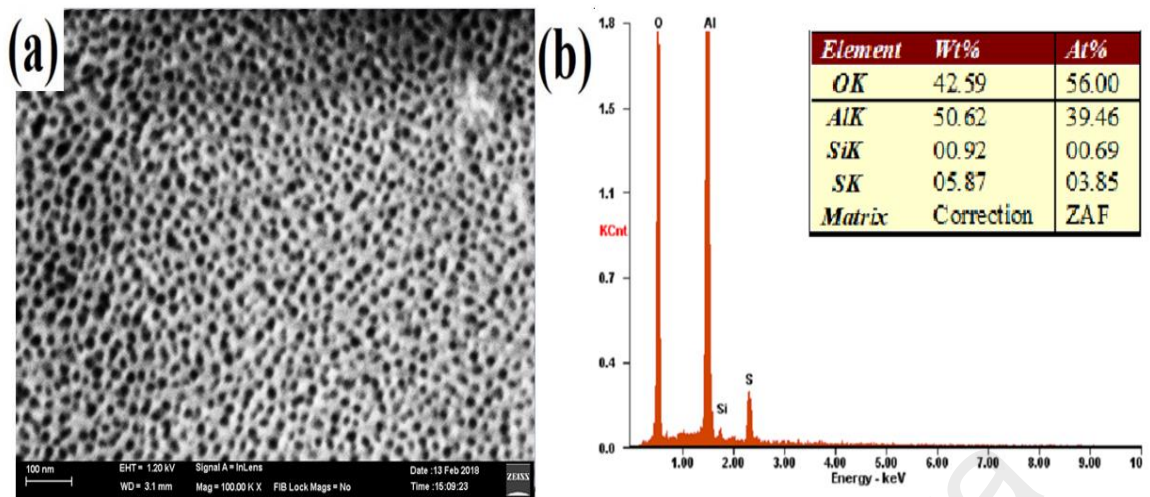


Figure 4.3: (a) FESEM top-view image and (b) EDX analysis of Al_2O_3 Nanoporous array after anodization for 1 h at 12 V in 15 wt% H_2SO_4

The effect of anodization duration on the thickness of AAO nanostructure coatings was determined using the FESEM cross-sectional view as shown in Figure 4.4. Based on this figure, it is observed that the thickness of the nanoporous alumina formed was approximated to be 500 nm. Correspondingly, a similar research was done by Chu *et al.* that by increasing the constant potential during anodization process, the pore orders located in the domain were also significantly improved (Chu *et al.*, 2005).

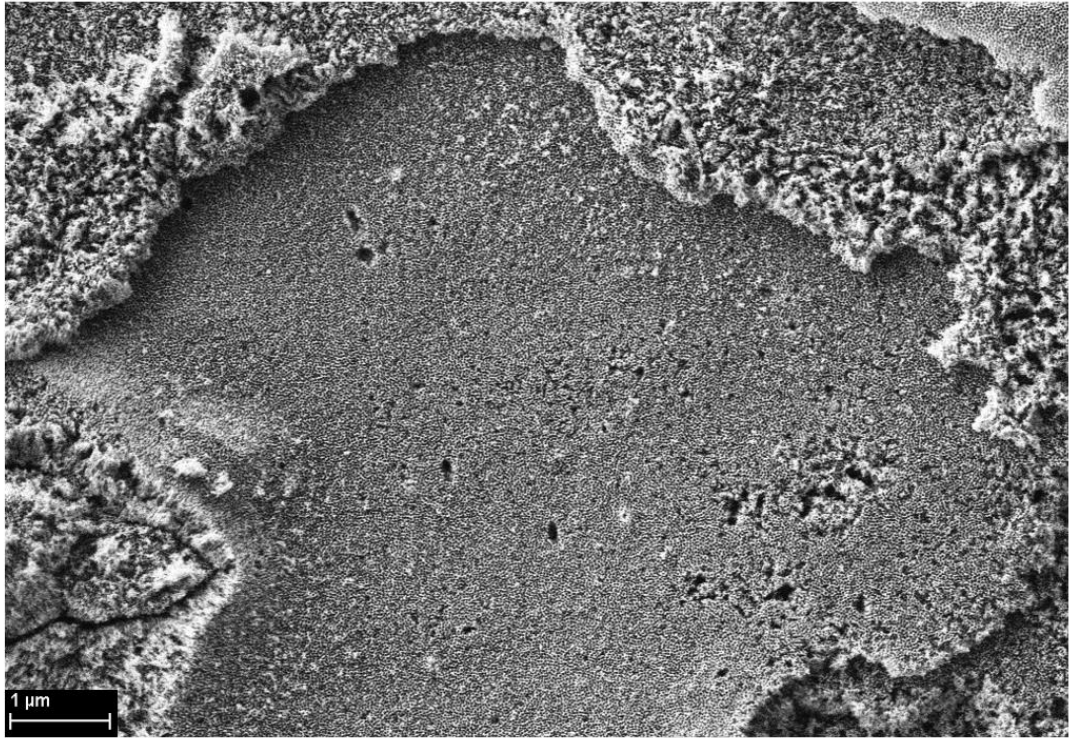


Figure 4.4: FESEM cross-sectional image of Al₂O₃ nanoporous array after anodization process for 1 h in an electrolyte containing 15 wt% H₂SO₄ at 12 V

4.3 Adhesion Strength of Al₂O₃ Nanoporous Array and Heat Treated

There are many factors that affects the adhesion strength of coatings such that surface pretreatments have been one of the key factor in the protection of aluminium alloy (Bajat *et al.*, 2008). The adhesion strength of AAO depends not only on the hardness of the oxide coating, but also on the durability and stability.

In this study, two experiments were carried out to improve the adhesion strength and consistency. Figure 4.5 shows the overall scratch track length and the failure point of the anodized coated sample. Figure 4.5 a-e illustrates the graph profiles of depth, load, friction force and coefficient of friction (COF) against distance, along with the failure points of the 1 h anodized specimen during the scratch force analysis. The scratch of the direction was done horizontally from left to right as shown in Figure 4.5a with a scratch

depth of ($\sim 1.8 \mu\text{m}$). Critical load was evaluated when the depth profile matched the delamination of coating. Therefore, critical load of the sample was attained from the load-distance graph profiles. As can be seen, the total scratch length of the anodized sample is $951.28 \mu\text{m}$, while the coating failure point was detected at $553.17 \mu\text{m}$. Aside from that, the adhesion strength of the coating increased to 1532 mN after anodization. Based on figure 4.5 d-e, the calculated friction and COF of anodized sample were calculated and plotted against the scratch length with both recorded at $1300 \mu\text{m}$ and 0.79 , respectively.

Figure 4.6 shows the adhesion strength of anodized alumina after underwent thermal treatment at $450 \text{ }^\circ\text{C}$ along with the scratch track length of $965.81 \mu\text{m}$ and the failure points recorded at $780.36 \mu\text{m}$ with an increased applied load of 2240 mN . As mentioned, Figure 4.6 b-e illustrates the scratch depth of ($\sim 2.5 \mu\text{m}$), a scratch load recorded at 2240 mN after heat treated, friction force of $1800 \mu\text{m}$ and COF against distance 0.75 , individually.

Based on the consolidated results attained from Figure 4.5 and 4.6, it can be observed that the longer optical micrograph scratch track has the best adhesion strength. The scratch failure showed an increase in the scratch track failure point after undergoing heat treatment. There is also an increased in the recorded scratch profile, scratch load and friction force plotted against the scratch length from 1.8 to $2.5 \mu\text{m}$ depth, scratch load of 1532 to 2240 mN and an increase in friction force of 1300 to $1800 \mu\text{m}$. Both specimens stayed stable and revealed a COF value of 0.79 and 0.75 respectively.

This showed that the alumina nanoporous coating remained stable forming homogenous microstructure and a variation of grain size after undergoing heat treating process. Subsequently, these findings imply that subsequent heat treatment on the samples may have affected the adhesion strength of the AAO. The scratch hardness for as-anodized and heat treated sample values were 9.753 GPa and 14.26 GPa respectively. These imply that subsequent annealing process provides better adhesion than the untreated substrate.

University of Malaya

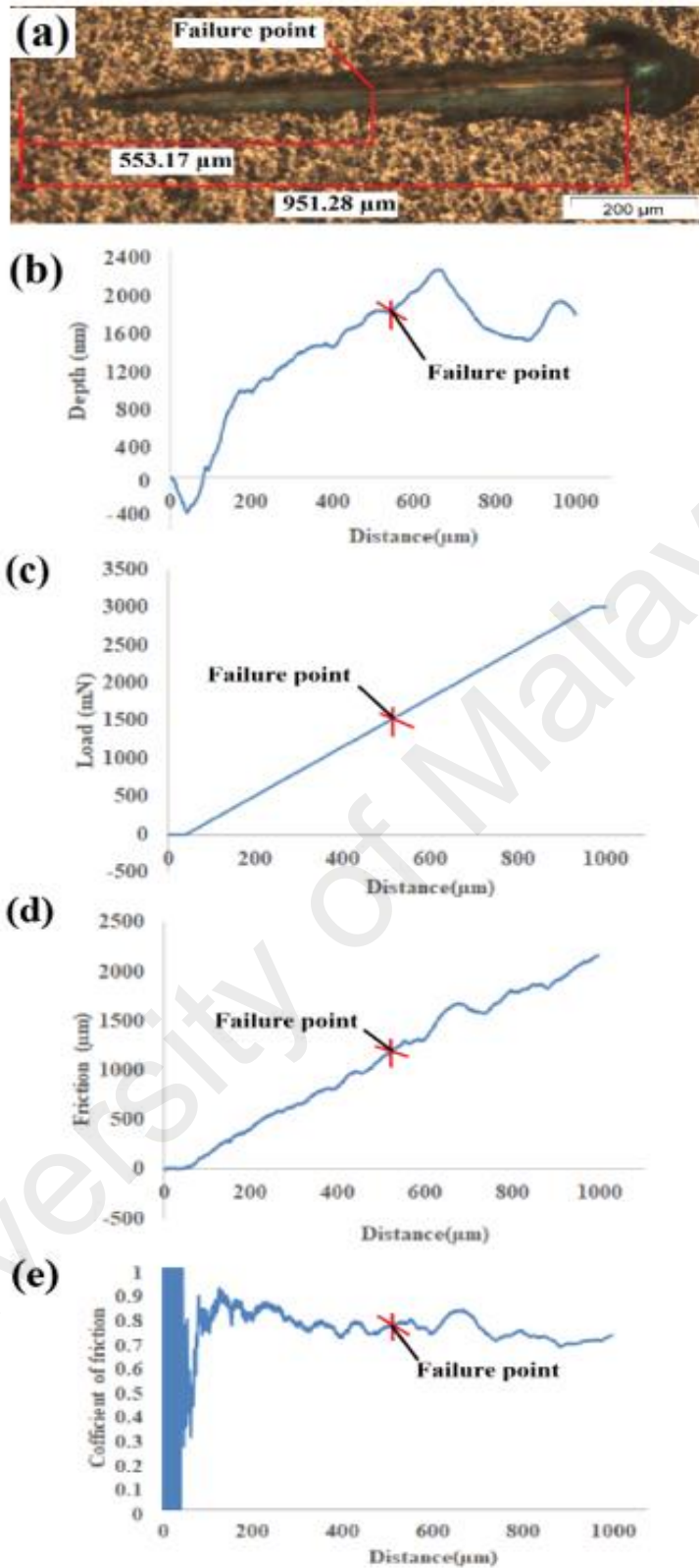


Figure 4.5: The optical micrograph of (a) scratch track and graph profiles of (b) depth, (c) load, (d) friction and (e) COF against scan distance inclusive of failure points of the 1 h anodized specimen

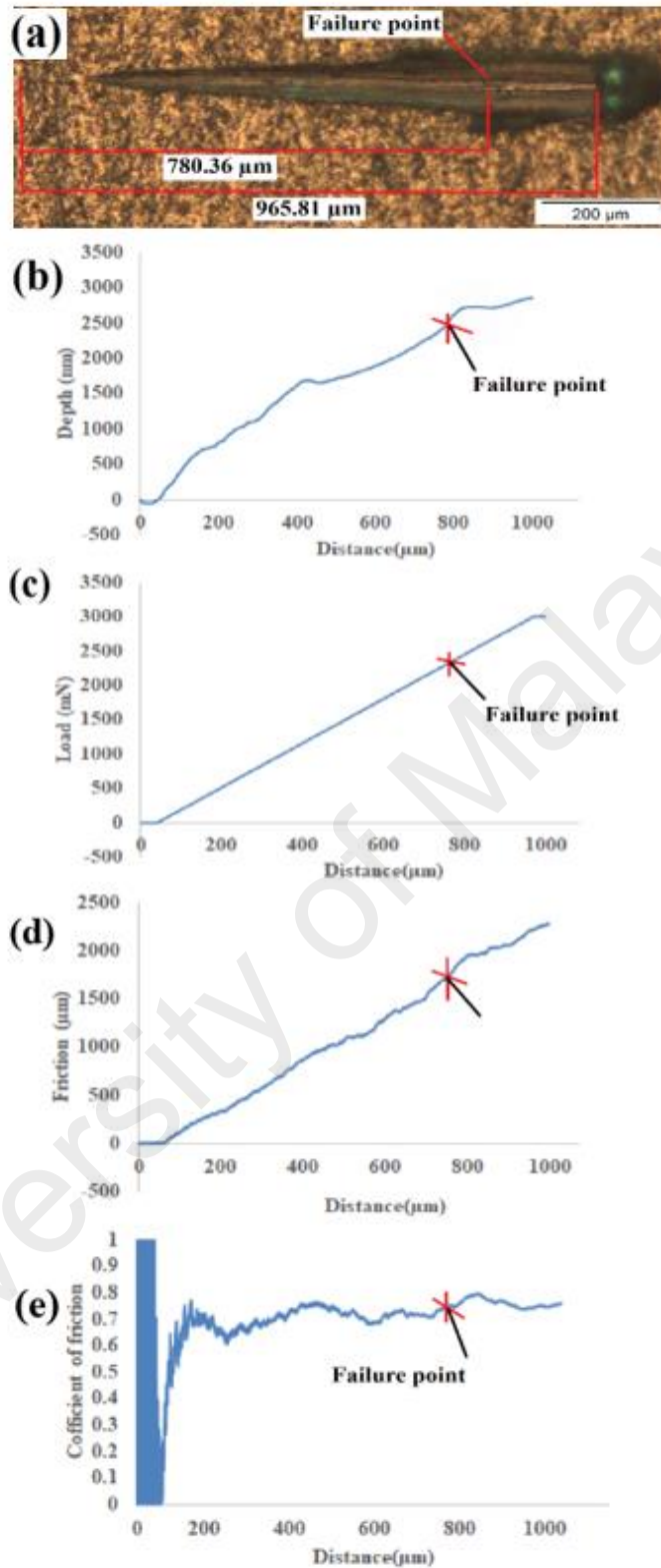


Figure 4.6: The optical micrograph of (a) scratch track and graph profiles of (b) depth, (c) load, (d) friction and (e) COF against scan distance inclusive of failure points for anodized sample after thermal heat treatment at 450 °C.

4.4 Vickers Microhardness

To reiterate, the surface hardness of coated oxide layer was determined by means of strength-indentation method using an applied load of 98.07 mN and dwell time of 15 s at ambient temperature. Table 4.7 shows the variation of Vickers hardness value for untreated substrate, un-annealed anodized sample, and finally the heat-treated sample at 450 °C. The hardness value of the substrate was 45.9 HV. After anodization, a nanoporous alumina layer was formed on the substrate; this effect increased the surface hardness value to 82.8 HV. Subsequently, after thermal annealing at 450 °C, a drop recorded in the surface hardness value of 71.2 HV but is still higher than the untreated substrate. The results obtained are justified by Zhang *et al.*, who reported that the surface hardness of each samples highly depends on the amount of porosity in each sample (Zhang *et al.*, 2006). The drop in hardness value from 82.8 to 71.2 HV after annealing at 450 °C showed that the precipitation hardening effect is being dominated by the softening effect after annealing. Rao and his co-workers researched that precipitates loses its coherency matrix, hence affecting the hardening effect. This can be concluded that the formation of equiaxed grains due to recrystallisation effect may have affected the strength and hardness of the as annealed sample while making it ductile (Rao *et al.*, 2013).

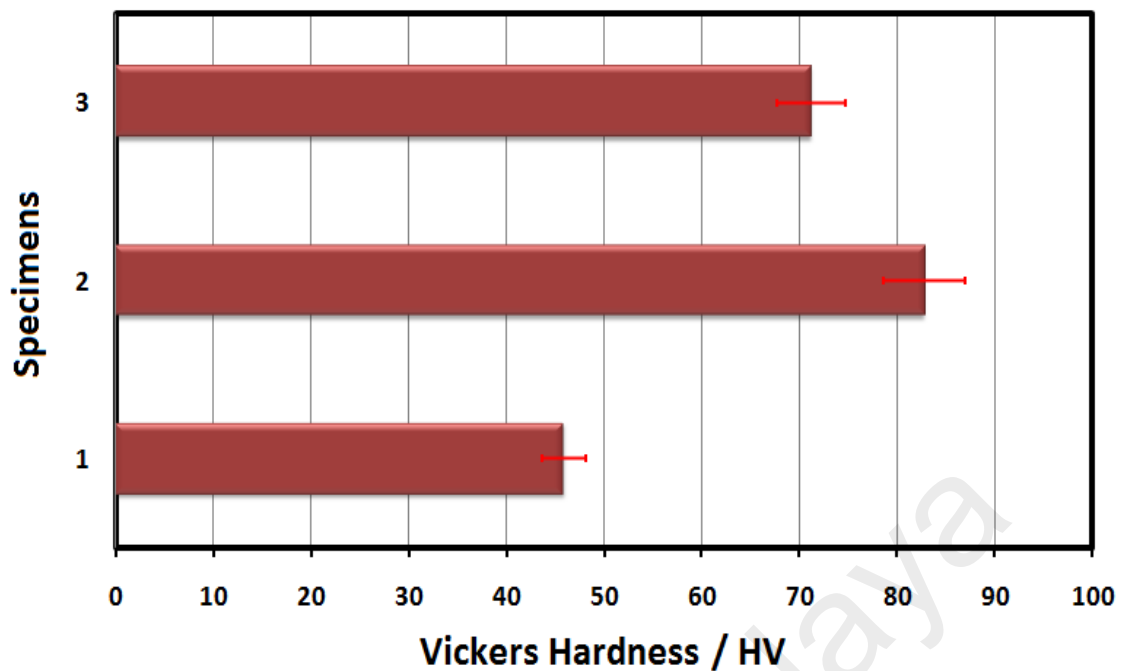


Figure 4.7: Vickers hardness value of (a) substrate, (b) anodization in 15 wt% H_2SO_4 and (c) heat treatment at 450 °C

4.5 Effectiveness of Corrosion Protection

Figure 4.8 illustrates the polarization plots of untreated substrate, Al_2O_3 as-anodized specimen and the 450 °C annealed sample. The values of E_{Corr} , I_{Corr} , R_p , and $P.E$ value are tabulated in Table 4.2. The AA substrate displayed a corrosion potential of -793 mV_{SCE} and corrosion current density of $9.023 \times 10^{-6} \mu A cm^{-2}$. For comparison, the as-anodized sample and heat treated recorded an increased in negative value indicating which indicates an increase in corrosion of the specimen. Besides that, the value of I_{Corr} slightly increased as the polarization curves moved towards the upper corrosion current density from a low of 9.023×10^{-6} to $1.313 \times 10^{-6} \mu A cm^{-2}$. The corrosion rate were determined for all three samples, which showed a decrease in corrosion activity of substrate at a rate of 3.91×10^{-6} , anodized sample at 2.72×10^{-6} and the annealed sample at 0.734×10^{-6} respectively. Last but not least, corrosion protection efficiencies were also

determined for all three samples. Through benchmarking, the anodized Al₂O₃ nanoporous array and annealed sample showed 46% and 85% increase in *P.E* individually against the bare substrate. It was noticed that the 450 °C had a significant improvement over *P.E* and exhibited the highest corrosion protection efficiency of 85%. According to Doodman *et al*, the heat treatment temperature also affects the corrosion properties of the coating surface (Doodman *et al.*, 2014). On a similar note, a research done by Dumitrascu *et al.* on anodized AA1050 showed that the E_{Corr} recorded a value of -440 mV_{SCE} with constant potential of 15 V. Likewise, by increasing the constant potential to 18 V, the E_{Corr} recorded a decrease in value to -550 mV_{SCE}. The decrease in similar trend could be related to the dissolution of boundary layers from the base of anodic oxide layers. Therefore, the increase in constant potential thickens the alumina layer and nanoporous diameter resulting in a more regulate order (Dumitrascu *et al.*, 2017).

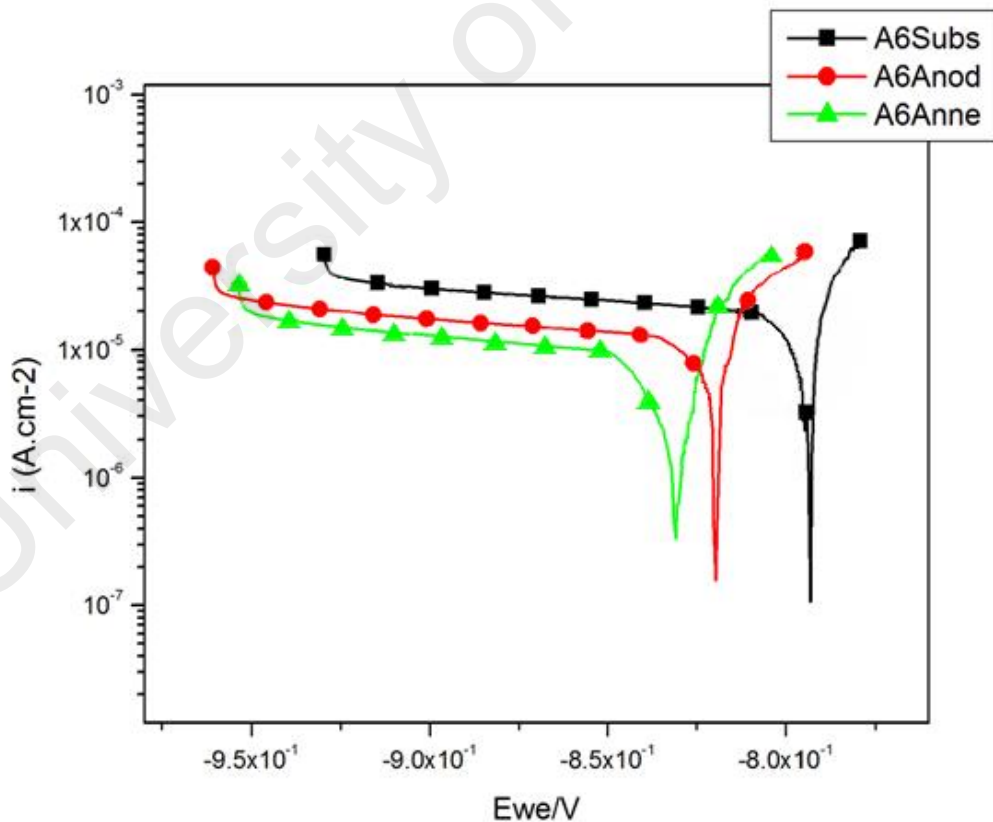


Figure 4.8: Polarization plots of the untreated substrate, the anodized specimen, and the 450 °C heat-treated sample.

Table 4.1: Corrosion potential (E_{Corr}), corrosion current density (I_{Corr}), corrosion rate and effectiveness of corrosion protection ($P.E.$) values

AA6061 S6	Substrate	Anodized	Annealing
$E_{\text{corr}} / (\text{mV}_{\text{SCE}})$	-793.753	-820.016	-830.946
$I_{\text{corr}} / \text{A}$ ($\mu\text{A cm}^{-2}$)	9.023×10^{-6}	4.858×10^{-6}	1.313×10^{-6}
Sample weight (g)	2.35	2.4	2.4
Density (g/cm ³)	2.7	3.95	3.95
E.W (g)	9	17	17
Corrosion rate	3.91×10^{-6}	2.72×10^{-6}	0.734×10^{-6}
$P.E$ (%)	-	46.16	85.45

4.6 Surface Wettability

The contact angle determines whether the surface is hydrophobic or hydrophilic. Figure 4.9 demonstrates the multiple WCA of substrate, the as-anodized sample in H_2SO_4 electrolyte, and heat treated sample of 450°C . It has been reported by Buijnsters *et al.* that the wetting of the AAO surface is highly dependent on the surface porosity (Buijnsters *et al.*, 2013). Low value of the contact angle indicates the high surface wettability. According to Figure 4.9a, the AA6061 bare substrate showed a contact angle of 95.7° , which caused by the hydrophobic surface. Based on the literature, the roughened solid surface tends to increase the contact angle due to the existence of air pocket between surface and liquid drop (Ran *et al.*, 2008). After anodization in 15 %wt H_2SO_4 for 1 h with constant voltage of 12 V, the contact value angle decreased significantly to 10.7° and 13.8° for both multiple sides as showed in Figure 4.9b. This suggest that the anodization is favorable in surface wettability. Figure 4.9c recorded the lowest

wetting contact angle of 7.7° , where the hydrophilic properties was improved after being heat treated at 450°C . Therefore, the surface modification of AA6061 by anodization and annealing proved to change the surface topography, roughness, composition and wettability (Kim *et al.*, 2006). It was reported by Ferro and Derby that the decrease in wetting angle after heat treatment is attributed to the formation of true metal and the breakup of alumina films. The combined effect of chemical reaction leads to the breakup of alumina films, hence leading with the formation of volatile aluminium oxide formed (Ferro & Derby, 1995).

University of Malaya

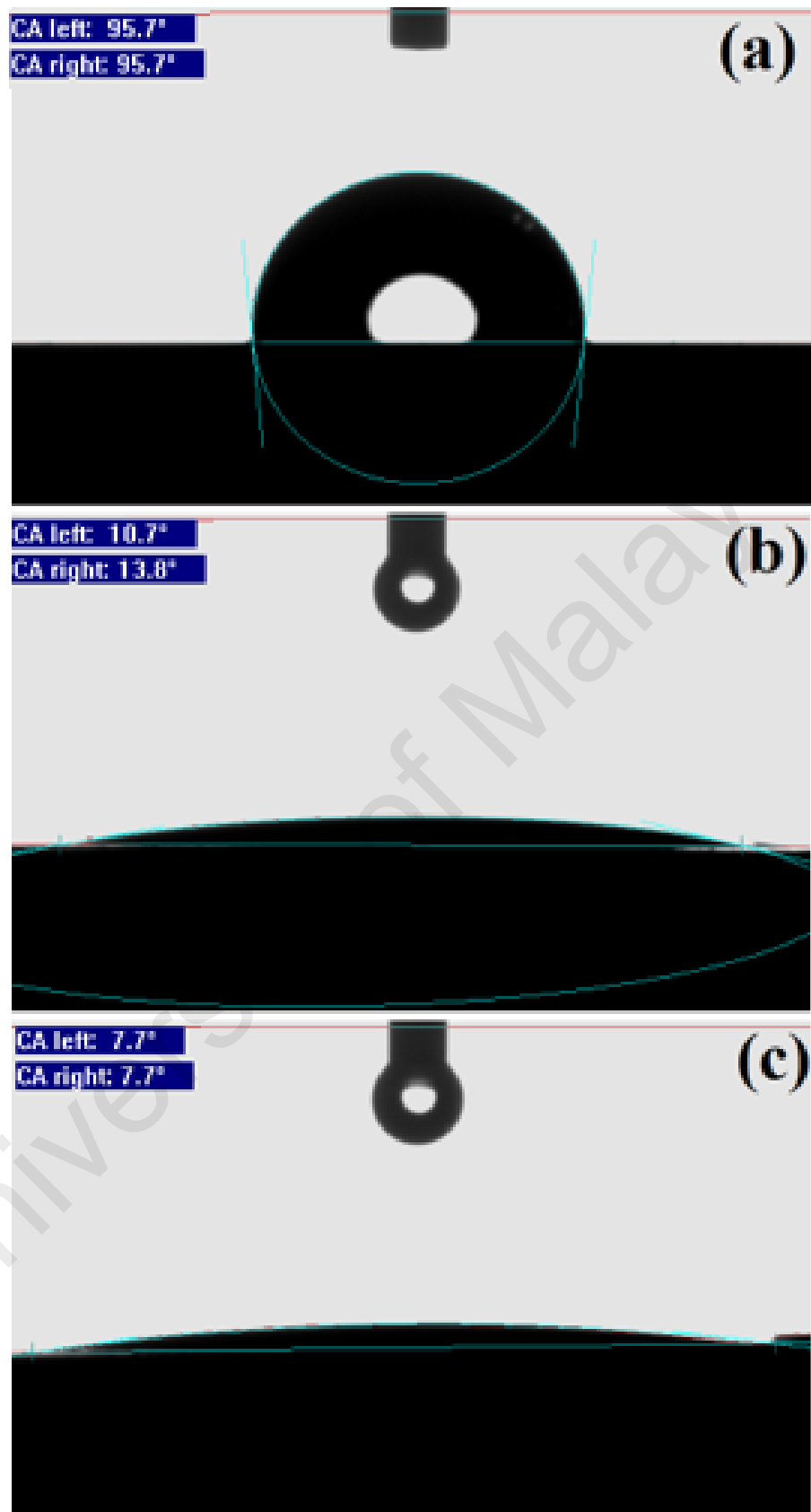


Figure 4.9: Optical images of the contact angle of (a) substrate, (b) anodized in H_2SO_4 electrolyte, and (c) heat treated sample at $450\text{ }^\circ\text{C}$.

CHAPTER 5: CONCLUSION AND FUTURE WORK

5.1 Conclusion

In the present work, nanoporous anodic alumina was successfully synthesized on aluminium alloy series 6 (AA6061 T657), followed by evaluation of mechanical and corrosion behavior in artificial salt water. A methodical investigation revealed an improved on the adhesion, surface hardness, scratch hardness, wear, corrosion resistance and wettability behavior between the substrate and film coating of nanoporous AAO.

According to the research, surface modification via anodization was done in an electrolyte containing 15% H₂SO₄ with constant potential of 12 V. It showed that the anodization process affects the topography due to the localized dissolution of the oxide layer. On top of that, the effect of anodization on the thickness of AAO nanostructure coatings was approximated to be 500 nm. Subsequently, it can be seen similarly that the surface modification via heat treatment also affects the adhesion strength of aluminium which recorded a scratch hardness value of 14.26 GPa against the as-anodized sample. Vickers hardness for anodization was also enhanced by anodization with a surface hardness value of 82.8 HV. Corrosion of AA6061 also indicated that the annealed sample showed significant improvement in the corrosion protection efficiency rate of 85% in ASW. Last but not least, surface wettability contact angle showed improved surface wettability (hydrophilicity) recorded at a contact angle of 7.7°.

Therefore, this project has demonstrated the feasibility of fabrication using AA6061 T657 for the production of nanoporous Al₂O₃ for both pre-treatment, and surface modification via anodization and heat treatment. This can be concluded that surface modification improved the mechanical and corrosion characteristics of AA6061. At the outset, this project has also met both of its objectives by investigating the corrosion behavior of AA6061 along with the microstructure analysis.

5.2 Suggestions for Future Work

The aim of this current research was to explore the nanoporous anodic alumina formed on aluminium alloy series 6 (AA6061 T657) for improved mechanical and corrosion behaviour. The evaluation of corrosion mechanism of this alloy in various corrosive media for different applications can also be investigated in future.

On top of that, anodizing by varying the potential voltage on the substrate may also determine the effect of particle size and distribution of fine crystalline particles relating to it. X-ray photoelectron spectroscopy (XPS) could be employed to determine further the elemental composition and surface chemistry of the formed Al_2O_3 .

University of Malaya

REFERENCES

- (2018). Retrieved from The Aluminium Association:
<https://www.aluminum.org/product-markets/automotive>
- Alwitt, R. S., McClung, R. C., & Jacobs, S. (1992). Anodized Aluminum Coatings for Thermal Control. *American Institute of Aeronautics and Astronautics*, 39-44.
- Anand S, S. T. (1997). Processing, Microstructure, and Fracture Behaviour of a Spray Atomized and Deposited Aluminium-Silicon Alloy. *Material Sciences* , 2835-2848.
- Association, E. A. (2018, October 7). Retrieved from Center for Advanced Automotive Technology : <http://autocaat.org/WebForms/ResourceDetail.aspx?id=1464>
- ASTM. (2003, April). Standard Test Method for Scratch Hardness of Materials Using a Diamond Stylus .
- Atkins, P., & Paula, J. D. (2009). *Elements of Physical Chemistry*. Great Britain : Oxford University Press.
- Bajat, J. B., Miskovic-Stankovic, V. B., & Kacarevic-Popovic, Z. (2008). Corrosion Stablility of Epoxy Coatings on Aluminium Pretreated by Vinyltriethoxysilane. *Corrosion Science*, 2078-2084.
- Ball, A. (1986). The Mechanisms of Wear, and the Performance of Engineering Materials. *South African Institute of Mining and Metallurgy*, 1-13.
- Bandyopadhyay, S., Miller, A. E., Chang, H. C., Banerjee, G., Yuzhakov, V., Yue, D. F., . . . Chandrasekhar, M. (1996). Electrochemically Assembled Quasi-Peridic Quantum Dot Arrays . *Nanotechnology*, 360-371.

- Barberoglou, M., Zorba, V., Pagozidis, A., Fotakis, C., & Stratakis, E. (2010). Electrowetting Properties of Micro/Nanostructured Black Silicon. *American Chemical Society*, 13007-13014.
- Beranek, R., Hildebrand, H., & Schmuki, P. (2003). Self-Organized Porous Titanium Oxide Prepared in H₂SO₄/HF Electrolytes. *Electrochemical and Solid-State Letters*, 12-14.
- Bidwell, J. P., & Spotte, S. (1985). Simulated Seawaters: Formulas and Methods. USA: Jones and Bartlett Publishers.
- Bocchetta, P., Sunseri, C., Masi, R., Piazza, S., & Di Quarto, F. (2003). Influence of Initial Treatments of Aluminium on the Morphological Features of Electrochemically formed Alumina Membranes. *Material Science and Engineering*, 1021-1026.
- Buijnsters, J. G., Zhong, R., Tsyntaru, N., & Celis, J. P. (2013). Surface Wettability of Macroporous Anodized Aluminium Oxide. *American Chemical Society*, 3224-3233.
- Chen, K. C., Liu, T. Y., & Chang, W. T. (2010). Effect of Oxalic Acid Concentration on the Formation of Anodic Aluminium Oxide using Pulse Anodization at Room Temperatures. *Microsys Technol*, 1451-1456.
- Chen, W., Wu, J. S., & Xia, X. H. (2008). Porous Anodic Alumina with Continuously Manipulated Pore/Cell Size. *ACS Nano*, 959-965.
- Cheng, T. C., & Chou, C. C. (2015). The Electrical and Mechanical Properties of Porous Anodic 6061-T6 Aluminium Alloy Oxide Film. *Journal of Nanomaterials*.

- Choi, J., Sauer, G., Nielsch, K., Wehrspohn, R. B., & Gosele, U. (2003). Hexagonally Arranged Monodisperse Silver Nanowires with Adjustable Diameter and High Aspect Ratio. *Chemical Material* , 776-779.
- Chou, S. N., Huang, J. L., Lii, D. F., & Lu, H. H. (2007). The Mechanical Properties and Microstructure of Al₂O₃/Aluminium Alloy Composites Fabricated by Squeeze Casting. *Journal of Alloy and Compounds*, 124-130.
- Chu, S. Z., Wada, K., Inoue, S., Isogai, M., & Yasumori, A. (2005). Fabrication of Ideally Ordered Nanoporous Alumina Films and Intergrated Alumina Nanotube Arrays by High-Field Anodization. *Advance Materials*, 2115-2119.
- Chu, S. Z., Wada, K., Inoue, S., Isogai, M., Katsuta, Y., & Yasumori, A. (2006). Large-Scale Fabrication of Ordered Nanoporous Alumina Films with Arbitrary Pole Intervals by Critical-Potential Anodization. *Electrochemical Socety*, 384-391.
- Chung, I. C., Chung, C. K., & Su, Y. K. (2017). Effect of Current Density and Concentration on Microstructure and Corrosion Behaviour of 6061 Al Alloy in Sulfuric Acid. *Surface and Coatings Technology* , 299-306.
- Cox, B. (1970). Factors Affecting the Groth of Porous Anodic Oxide Films on Zirconium. *Solid State Science*, 654-663.
- Curkovic, L., & Jelaca, M. F. (2009). Dissolution of Alumina Ceramics in HCl Aqueous Solution. *Ceramics International*, 2041-2045.
- Curkovic, L., Jelaca, M. F., & Kurajica, S. (2008). Corrosion Behavior of Alumina Ceramics in Aqueous HCl and H₂SO₄. *Corrosion Science*, 872-878.

De Azevedo, W. M., Carvalho, D. D., Khoury, H. J., de Vasconcelos, E. A., & da Silva, E. F. (2004). Spectroscopic Characteristic of Doped Nanoporous Aluminium Oxide. *Materials Science Engineering*, 171-174.

Diggle, J. W., Downie, T. C., & Goulding, C. W. (1968). Anodic Oxide Films on Aluminum. *Chemical Review*, 365-405.

Dohda, K. B.-A. (2015). Tribology in metal forming at elevated temperatures. *Friction*, 3-23.

Doodman, P., Faghihi-Sani, M. A., Barati, N., & Afshar, A. (2014). Alumina Nanostructured Coating for Corrosion Protection of 316L Stainless Steel. *J. Nano Dimens*, 27-33.

Doty, H. W. (2005). *United States Patent No. US 6,921,512 B2*.

Du, X., & Xu, Y. (2008). Formation of Al₂O₃-BaTiO₃ Composite Thin Film to Increase the Specific Capacitance of Aluminium Electrolytic Capacitor. *Thin Solid Films*, 8436-8440.

Dumitrascu, V., Benea, L., & Danaila, E. (2017). Corrosion Behavior of Aluminium Oxide Film Growth by Controlled Anodic Oxidation. *International Conference on Innovative Research*, 1-7.

Dutrow, B. L., & Clark, C. M. (2018, November 4). *Carleton College*. Retrieved from X-Ray Powder Diffraction (XRD): https://serc.carleton.edu/research_education/geochemsheets/techniques/XRD.html

- El-Hameed, A. M., Abdel-Haziz, Y. A., & El-Tokhy, F. S. (2017). Anodic Coating Characteristics of Different Aluminium Alloys for Spacecraft Materials Applications. *Materials Sciences and Applications*, 197-208.
- Elias, C. N., Oshida, Y., Lima, J. H., & Muller, C. A. (2008). Relationship between Surface Properties (Roughness, Wettability, Morphology) of Titanium and Dental Implant Removal Torque. *Mechanical Behavior of Biomedical Materials*, 234-242.
- Ferro, A. C., & Derby, B. (1995). Wetting Behaviour in the Al-Si/SiC System: Interface Reactions and Solubility Effects. *Elsevier Science Ltd*, 3061-3073.
- Fournier, S. B., Kitaev, V., Routkevitch, D., Manners, I., & Ozin, G. A. (2004). Highly Ordered Nanosphere Imprinted Nanochannel Alumina (NINA). *Advanced Materials*, 2193-2196.
- Goldstein, J. I., Newbury, D. E., Echlin, P., Joy, D. C., Lyman, C. E., Lifshin, E., . . . Michael, J. R. (1981). *Scanning Electron Microscopy and X-Ray Microanalysis*. New York: Plenum.
- Gonzalez, J. A., Lopez, V., Bautista, A., & Otero, E. (1999). Characterization of Porous Aluminium Oxide Films from A.C Impedance Measurements. *Applied Electrochemistry*, 229-238.
- Grubbs, C. A. (1999). Anodizing of Aluminium. *J. Metal Finishing*, 480-496.
- Hao, L., & Cheng, R. B. (2000). Sealing Processes of Anodic Coatings - Past, Present, and Future. *METALAST International Inc.*, 8-18.

- Huang, M. H., Wu, Y., Feick, H., Tran, N., Weber, E., & Yang, P. (2001). Catalytic Growth of Zinc Oxide Nanowires by Vapor Transport. *Advanced Materials*, 113-116.
- Ikonopisov, S., Girginov, A., & Machkova, M. (1979). Electrical Breaking Down of Barrier Anodic Films During Their Formation. *Electrochimica Acta* , 451-496.
- Ilango, M. S., Mutalikdesai, A., & Ramasesha, S. K. (2016). Anodization of Aluminium Using a Fast Two-Step Process. *Indian Academy Sciences*, 153-158.
- Jaworski, R., Pawlowski, L., Roudet, F., Kozerski, S., & Petit, F. (2008). Characterization of Mechanical Properties of Suspension Plasma Sprayed TiO₂ Coatings using Scratch Test. *Surface & Coatings Technology*, 2644-2653.
- Jessensky, O., Muller, F., & Gosele, U. (1998). Self-Organized Formation of Hexagonal Pore Arrays in Anodic Alumina. *American Institute of Physics*, 1173-1175.
- Jessensky, O., Muller, F., & Gosele, U. (1998). Self-Organized Formation of Hexagonal Pore Structures in Anodic Alumina. *Electrochemical Society*, 3735-3740.
- Jiang, C. X., Guo, S. Y., Tu, J., & Fu, M. F. (2005). Friction Properties of Oil-Infiltrated Porous AAO Film on Aluminium Substrate. *Acta Metallurgica Sinica (English Letters)*, 249-253.
- Kao, T. T., & Chang, Y. C. (2014). Influence of Anodization Parameters on the Volume Expansion of Anodic Aluminium Oxide Formed in Mixed Solution of Phosphoric and Oxalic Acids. *Applied Surface Science*, 654-659.
- Kashi, M. A., Ramazani, A., Rahmandoust, M., & Noormohammadi, M. (2007). The Effect of pH and Composition of Sulfuric-Oxalic Acid Mixture on the Self-

Ordering Configuration of High Porosity Alumina Nanohole Arrays. *Applied Physics*, 4625-4630.

Kasuga, T., Hiramatsu, M., Hoson, A., Sekino, T., & Niihara, K. (1992). Formation of Titanium Oxide Nanotube . *American Chemical Society*, 3160-3163.

Keller, F., Hunter, M. S., & Robinson, D. L. (1953). Structural Features of Oxide Coatings on Aluminium. *Electrochemical Society*, 411-419.

Kikuchi, T., Nakajima, D., Nishinaga, O., Natsui, S., & Suzuki, R. O. (2015). Porous Aluminium Oxide Formed by Anodizing in Various Electrolyte Species. *Current Nanoscience*, 560-571.

Kikuchi, T., Yamamoto, T., & Suzuki, R. O. (2013). Growth Behavior of Anodic Porous Alumina Formed in Malic Acid Solution. *Applied Surface Sciences* , 907-913.

Kim, S. J., Bang, I. C., Buongiorno, J., & Hu, L. W. (2006). Effects of Nanoparticle Deposition on Surface Wettability Influencing Boiling Heat Transfer in Nanofluids. *American Institute of Physics*, 1-3.

Kucharikova, L., Liptakova, T., Tillova, E., Kajanek, D., & Schmidova, E. (2018). Role of Chemical Composition in Corrosion of Aluminium Alloys. *Metals*, 3-13.

Landmark, A. (2005). *Siegfried Marcus Car*. Retrieved from <https://www.asme.org/about-asme/who-we-are/engineering-history/landmarks/203-siegfried-marcus-car>

Lee, G. S., Choi, J. H., Choi, Y. C., Bu, S. D., & Lee, Y. Z. (2011). Tribological Effects of Pores on an Anodized Al Alloy Surface as Lubricant Reservoir. *Current Applied Physics*, 182-186.

- Lee, W., & Park, S. J. (2014). Porous Anodic Aluminium Oxide: Anodization and Templated Synthesis of Functional Nanostructures. *Chemical Reviews*, 7487-7556.
- Li, D. J. (2009). Scratch Hardness Measurement using Mechanical Tester. California, Irvine, United States of America.
- Li, K. e. (2013). Evolution of near-surface deformed layers on AA3104 aluminum alloy. *Material Science* , 358-362.
- Lim, S. L. (2011). Aluminium Oxide Template And Titanium Oxide Nanotubes and Their Applications. 20-141.
- Liu, B. e. (2017). The corrosion behaviour of machined AA7150-T651 aluminum alloy. *Corrosion Science*, 2.
- Masuda, H., & Fukuda, K. (1995). Ordered Metal Nanohole Arrays Made by a Two-Step Replication of Honeycomb Structures of Anodic Alumina. *Science*, 1466-1468.
- Masuda, H., & Hasegawa, F. (1997). Self-Ordering of Cell Arrangement of Anodic Porous Alumina Formed in Sulfuric Acid Solution. *J. Electrochem. Soc.*
- Masuda, H., Yada, K., & Osaka, A. (1998). Self-Ordering of Cell Configuration of Anodic Porous Alumina with Large-Size Pores in Phosphoric Acid Solution. *Japan Applied Physics*, 1340-1342.
- Masuda, H., Yotsuya, M., Asano, M., Nishio, K., Nakao, M., Yokoo, A., & Tamamura, T. (2001). Self-Repair of Ordered Pattern of Nanometer Dimensions Based on Self-Compensation Properties of Anodic Porous Alumina. *American Institute of Physics*, 826-828.

- Milak, P. C., Minatoo, F. D., De Noni, A., & Montedo, O. R. (2015). Wear Performance of Alumina-Based Ceramics - A Review of the Influence of Microstructure on Erosive Wear. *Ceramica*, 88-103.
- Miller, W. S., Zhuang, L., Bottema, J., Witterbrood, A. J., De Smet, P., Haszler, A., & Vieregge, A. (2000). Recent Development in Aluminium Alloys for the Automotive Industry. *Material Science and Engineering*, 37-49.
- Mor, G. K., Varghese, O. K., Paulose, M., Mukherjee, N., & Grimes, C. A. (2003). Fabrication of tapered, conical-shaped Titania Nanotubes. *Materials Research Society*, 2588-2593.
- Morita, A. (1998). Aluminium Alloys for Automobiles Applications. *Aluminium Alloys*, 25-32.
- Mozalev, A., Bendova, M., Guirado, F. G., Pytlíček, Z., & Llobet, E. (2016). Metal-Substrate-Supported Tungsten Oxide Nanoarrays via Porous-Alumina-Assisted Anodization: From Nanocolumns to Nanocapsules and Nanotubes. *Materials Chemistry*, 8219-8232.
- Nayak, S. (2004). Laser Induced Surface Modification of Aluminium Alloys. 15-170.
- Ono, S., Saito, M., Ishiguro, M., & Asoh, H. (2004). Controlling Factor of Self-Ordering of Anodic Porous Alumina. *Electrochemical Society*, 473-478.
- O'Sullivan, J. P., & Wood, G. C. (1970). The Morphology and Mechanism of Formation of Porous Anodic Films on Aluminium. *Proceeding of the Royal Society London*, 511-541.

- Parkhutik, V. P., & Shershulsky, V. I. (1992). Theoretical Modelling of Porous Oxide Growth on Aluminium. *Journal of Applied Physics*, 1258-1263.
- Prasad B.K, V. K. (1998). Sliding Wear Behavior of Some Al-Si Alloys: Role of Shape and Size of Si Particles and Test Conditions. *Metallurgical and Materials Transactions*, 2747-2752.
- Quazi, M. M. (2015). Laser-based Surface Modifications of Aluminium and its Alloys . *Solid State and Materials Science* , 2-21.
- Rahimi, M. H., Tabaian, S. H., Hoveyda Marashi, S. P., Amiri, M., & Dalaly, M. M. (2008). The Effect of Aluminium Electropolishing on Nano-Pores Arrangement in Anodic Alumina Membranes. *Journal of Modern Physics B*, 3267-3277.
- Ran, C., Ding, G., Liu, W., Deng, Y., & Hou, W. (2008). Wetting on Nanoporous Alumina Surface: Transition between Wenzel and Cassie States Controlled by Surface Structure. *American Chemical Society*, 9952-9955.
- Rao, P. N., Singh, D., & Jayaganthan, R. (2013). Effect of Annealing on Microstructure and Mechanical Properties of Al 6061 Alloy Processed by Cryorolling. *Material Science and Technology*, 76-82.
- Research and Markets*. (2018, April 24). Retrieved from https://www.researchandmarkets.com/research/c2s372/high_strength?w=4
- Revie, R. U. (2008). *Introduction to Corrosion Science and Engineering*. New Jersey: John Wiley & Sons Inc.
- Rodrigues, S. (2017). Water and oil wettability of anodized 6016 aluminium alloy surface. *Applied surface sciences*, 430-442.

Rulik, L. (2014, May). Surface Studies on Industrial Aluminium Alloy. Sweden.

Runge, J. (1999). Impact of Surface Treatment & Interfacial Phenomena on the Anodizing Process. *CompCote International*, 1-20.

Runge, J. M., & Pomis, A. J. (2000, March). Anodic Oxide Film Formation Relating Mechanism to Composition and Structure. USA, Illinois.

Sarhan, Z. H. (2013). The Influence of Higher Surface Hardness on Fretting Fatigue Life of Hard Anodized Aerospace AL7075-T6 Alloy. *Material Science & Engineering*, 377-387.

Sarikaya, O. (2005). Effect of Some Parameters on Microstructure and Hardness of Alumina Coatings Prepared by Air Plasma Spraying Process. *Surface & Coating Technology*, 388-393.

Schacht, M., Boukis, N., & Dinjus, E. (2000). Corrosion of Alumina Ceramics in Acidic Aqueous Solutions at High Temperatures and Pressures. *Journal of Material Sciences*, 6251-6258.

Shahzad, M., Chaussimier, M., Chieragatti, R., Mabru, C., & Aria, F. R. (2011). Surface Characterization and Influence of Anodizing Process on Fatigue Life of Al 7050 Alloy. *Materials and Design*, 3328-3335.

Shingubara, S., Morimoto, K., Sakaue, H., & Takahagi, T. (2004). Self-Organization of a Porous Alumina Nanohole Array Using a Sulfuric/Oxalic Acid Mixtures as Electrolyte. *Electrochemical and Solid State Letters*, 15-17.

- Sieber, I., Hildebrand, H., Friedrich, A., & Schmuki, P. (2005). Formation of Self-Organized Niobium Porous Oxide on Niobium. *Electrochemistry Communications*, 97-100.
- Sieber, I., Kannan, B., & Schmuki, P. (2005). Self-Assembled Porous Tantalum Oxide Prepared in H₂SO₄/HF Electrolytes. *Electrochemical and Solid-State Letters*, 10-12.
- Su, Z., & Zhou, W. (2009). Porous Anodic Metal Oxides. *Science Foundation in China*, 36-53.
- Tacconi, N. R., Chenthamarakshan, C. R., Yogeewaran, G., Watcharenwong, A., De Zoysa, R. S., Basit, N. A., & Rajeshwar, K. (2006). Nanoporous TiO₂ and WO₃ Films by Anodization of Titanium and Tungsten Substrates: Influence of Process Variables on Morphology and Photoelectrochemical Response. *American Chemical Society*, 25347-25355.
- Thompson, G. E. (1997). Porous Anodic Alumina: Fabrication, Characterization, and Applications. *Thin Solid Films*, 192-201.
- Thompson, G. E., Furneaux, R. C., Wood, G. C., Richardson, J. A., & Goode, J. S. (1978). Aluminium, Nucleation and Growth of Porous Anodic Films on Aluminium. *Macmillan Journals*, 433-435.
- Tsuchiya, H., & Schmuki, P. (2005). Self-Organized High Aspect Ratio Porous Hafnium Oxide prepared by Electrochemical Anodization. *Electrochemistry Communications*, 49-52.

- Tsuchiya, H., Macak, J. M., Sieber, I., & Schmuki, P. (2005). Self-Organized High-Aspect Ratio Nanoporous Zirconium Oxides Prepared by Electrochemical Anodization. *Nanoporous Materials*, 722-725.
- Tuscharoen, S., Pokai, S., Horprathum, M., Limnonthakul, P., Eiamchai, P., Pattantsetakul, V., . . . Kaewkhao, J. (2017). Wetting Characteristic of Nanoporous Aluminium Oxide Films. *Materials Today: Proceedings*, 6615-6619.
- Uchi, H., Kanno, T., & Alwitt, R. S. (2001). Structural Features of Crystalline Anodic Alumina Films. *Electrochemical Society*, 17-23.
- Vatne, H. E., Engler, O., & Nes, E. (1994). The Effect of Precipitates on Texture Development. *Texture of Materials*, 1501-1506.
- Wang, J., Wang, C. W., Li, Y., & Liu, W. M. (2008). Optical Constants of Anodic Aluminium Oxide Films Formed in Oxalic Acid Solution. *Thin Solid Films*, 7689-7694.
- Westre, T., Cheng, B. R., Hao, L., & Westre, S. (2000). Performance Results for Sealed Type III Anodic Oxides. *AESF SUR/FIN*.
- Wood, G. C., Skeldon, P., Thompson, G. E., & Shimizu, K. (1996). A Model for the Incorporation of Electrolyte Species into Anodic Alumina. *The Electrochemical Society*, 74-82.
- Wu, Z., Richter, C., & Menon, L. (2007). A Study of Anodization Process during Pore Formation in Nanoporous Alumina Templates. *Electrochemical Society*, 8-12.

- Xhanari, K., & Finsgar, M. (2016). Organic Corrosion Inhibitors for Aluminium and Its Alloys in Chloride and Alkaline Solutions: A review. *Arabian Journal of Chemistry*.
- Xu, D., Xu, Y., Chen, D., Gui, G., Gui, L., & T. Y. (2010). Preparation of CdS Single-Crystal Nanowires by Electrochemically Induced Deposition. *Advanced Materials*, 520-522.
- Yahalom, J., & Hoar, T. P. (1970). Galvanostatic Anodizing of Aluminium. *Electrochimica Acta*, 877-884.
- Yi Li, H. S., Sakairi, M., Shigyo, K., Takahashi, H., & Seo, M. (1997). Formation and Breakdown of Anodic Oxide Films on Aluminium in Boric Acid/Borate Solutions. *Electrochemical Society*, 866-876.
- Young, L. (1960). Steady-State Kinetics of Formation of Anodic Oxide Films on Tantalum in Sulphuric Acid. *The Royal Society*, 496-515.
- Yu, Y. H., Lin, Y. Y., Lin, C. H., Chan, C. C., & Huang, Y. C. (2014). High-Performance Polystyrene-/Graphene-Based Nanocomposites with Excellent Anti-Corrosion Properties. *Polymer Chemistry*, 535-550.
- Yuan, S., Liang, B., Zhao, Y., & Pehkonen, S. O. (2013). Surface Chemistry and Corrosion Behaviour of 304 Stainless Steel in Simulated Seawater containing Inorganic Sulphide and Sulphate-Reducing Bacteria. *Corrosion Science*, 1-14.
- Yudong, L. (2017). Research Progress in Formation Mechanism of Anodizing Aluminium Oxide. *1st International Global on Renewable Energy and Development (IGRED 2017)* (pp. 1-6). IOP Publishing.

- Zaraska, L., Sulka, G. D., & Jaskula, M. (2010). Porous Anodic Alumina Membranes Formed by Anodization of AA1050 Alloy as Templates for Fabrication of Metallic Nanowire Arrays. *Surface and Coatings Technology*, 2432-2437.
- Zhang, J., Kielbasa, J. E., & Carroll, D. L. (2010). Controllable Fabrication of Porous Alumina Templates for Nanostructures Synthesis . *Material Chemistry and Physics*, 295-300.
- Zhang, Y., Chen, J., Hu, L., & Liu, W. (2006). Pressureless-Sintering Behavior of Nanocrystalline ZrO₂-Y₂O₃-Al₂O₃ System . *Materials Letters*, 2302-2305.
- Zhao, N. Q., Jiang, X. X., Shi, C. S., Li, J. J., Zhao, Z. G., & Du, X. W. (2007). Effects of Anodizing Conditions on Anodic Alumina Structure. *Journal of Material Science*, 3878-3882.
- Zhao, S., Chan, K., Yelon, A., & Veres, T. (2007). Novel Structure of AAO Film Fabricated by Constant Current Anodization. *Advanced Materials* , 3004-3007.